CONTRIBUTION TO THE PHYSICAL MODELING OF THE CIRCULATORY SYSTEM

OPTIMIZATION AND EVOLUTION

Carla Alexandra de Castro Carvalho e Silva

Tese apresentada à Universidade de Évora
para obtenção do Grau de Doutor em Física
Especialidade: Física

ORIENTADOR: *Professor Doutor António Domingos Heitor da Silva Reis*

ÉVORA, DEZEMBRO 2014

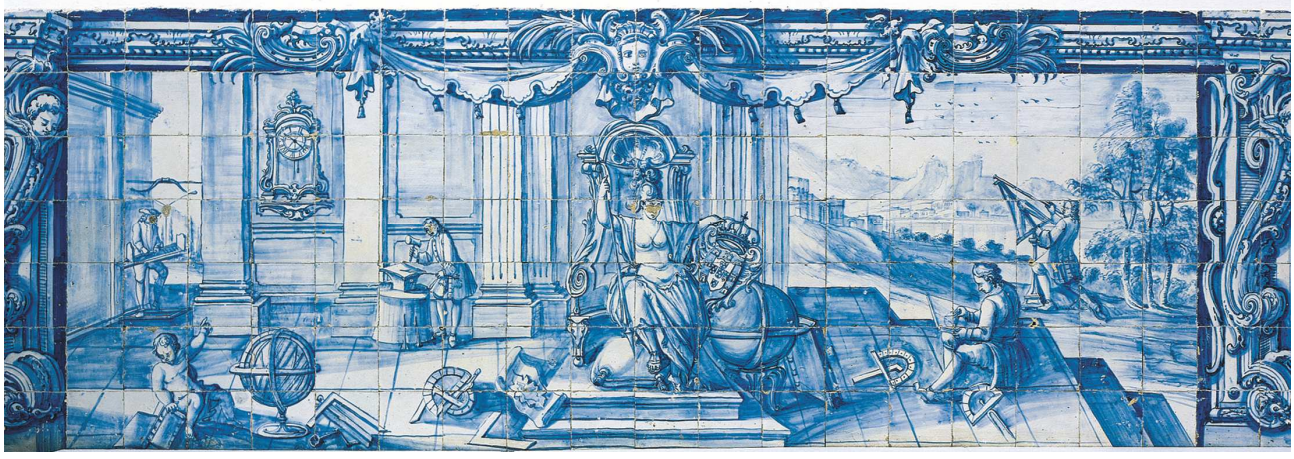

INSTITUTO DE INVESTIGAÇÃO E FORMAÇÃO AVANÇADA

Summary

Branched networks are ubiquitous in living systems. The dimensions and the geometry of these branched structures are key aspects of the efficiency of physiological processes. A resistive-capacitive model of an optimized pulsatile flow system based on Constructal Theory is presented, which aims to explain the performance of the human arterial tree. Optimal scaling laws for diameters and lengths emerged that are valid for dichotomous branching. The model together with data of the human arterial tree showed that impedances of some arteries tend to decrease with age. The estimated scaling between diameters of branching arteries is close to optimality. With respect to scaling of arterial length no such agreement was observed. An interpretation of the lifelong elongation of the ascending aorta is proposed. The model together with Starling equation, continuity of blood flow, and the specific properties of the exchanges in capillaries provide an explanation for the observed reduction of arterial distensibility with pulse frequency observed in carotid and radial arteries.

Resumo

Contribuição para a modelação física do sistema circulatório - Optimização e evolução

As redes ramificadas estão presentes nos sistemas vivos. As dimensões e a geometria dessas estruturas ramificadas são aspectos chave da eficiência dos processos fisiológicos. É apresentado um modelo resistivo-capacitivo de um sistema de escoamento pulsado optimizado com base na Teoria Constructal, com o objectivo de explicar a performance da rede arterial humana. São obtidas leis de escala óptima para diâmetros e comprimentos, válidas para ramificações dicotómicas. A associação do modelo com dados da rede arterial humana revelou que a impedância de algumas artérias tende a diminuir com a idade. A razão das escalas entre os diâmetros estimados das artérias apresenta valores quase optimizados. O mesmo não foi observado relativamente às leis de escala dos comprimentos das artérias. É proposta uma interpretação para o alongamento da aorta ascendente ao longo da vida. O modelo desenvolvido juntamente com a equação de Starling, a continuidade do fluxo sanguíneo, e as propriedades específicas das trocas nos capilares, permitem explicar a redução da distensibilidade arterial com a pulsação observada nas artérias carótida e radial.

Acknowledgements

I would like to thank my supervisor Professor António Heitor Reis for his endless support and guidance throughout this thesis.

I acknowledge the support of the Geophysics Centre of Évora (CGE) and of the Physics Department of the University of Évora for providing me the conditions to the development of this work. I also acknowledge the funding provided by the CGE, under the contracts with FCT (the Portuguese Science and Technology Foundation), Pest/OE/CTE/UI0078/2011 and Pest/OE/CTE/UI0078/2014.

I thank my family for the valuable and crucial support. This work would not have been possible without their contribution.

Contents

Nomenclature

A	vessel cross sectional area (m^2)
A_0, A_1, A_2	channels parameter (page 38)
a_K	parameter (page 75)
B	parameter (page 38) (m^3)
b	allometric scaling exponent (Eq. 1.1)
C	channel compliance (Pa^{-1} m^3)
D, D_0, D_1, D_2	channels diameter (m)
D_{us}, D_{0us}, D_{1us}, D_{2us}	unstrained channels diameter (page 42) (m)
I	flow rate (m^3 s^{-1})
i_i	interstitial space current (m^3 s^{-1})
i_{ci}	net current from the capillary to the interstitial space (m^3 s^{-1}) (page 72)
i_{lymph}	lymphatic current (Eq. 4.6) (m^3 s^{-1})
I_r	resistive current (Eq. 2.5) (m^3 s^{-1})
I_{cap}	capacitive current (Eq. 2.6) (m^3 s^{-1})
I_c	capillary current (Eq. 4.2) (m^3 s^{-1})
i_v	venular end current (Eq. 4.4) (m^3 s^{-1})
K	conductance (Pa^{-1} s^{-1} m^3)
k, k_0, k_1, k_2	channels parameter (Eq. 2.10) (s)
k_A	constant (page 17) (Pa s)
k_B	constant (page 24) (Pa^{-1})
k_{ci}	filtration coefficient from the capillary side (page 72) (Pa^{-1} m^3 s^{-1})
k_{ic}	filtration coefficient from the interstitial space side (page 73) (Pa^{-1} m^3 s^{-1})
L, L_0, L_1,L_2	channels length (m)
L_c	characteristic length (m)
M	mass (kg)
N	number of branching levels
P	pressure (Pa)
P_a	pressure at the end of the arteriole (Pa)
P_c	capillary pressure (Pa)

P_i	interstitial space pressure (Pa)
P_v	pressure at the beginning of the venule (Pa)
R	flow resistance (kg m^{-4} s^{-1})
R_e	Reynolds number
$\dot{s}_{gen}$	entropy generation rate (W K^{-1})
T	thermodynamic temperature (K)
u	mean velocity (m s^{-1})
V	channel volume (m^3)
$\tilde{V}$	reduced volume $\tilde{V} = 4V/\pi$ (m^3)
X_c	capacitive reactance (kg m^{-4} s^{-1})
y	parameter (page 37)
Y	biological parameter (Eq. 1.1)
Y_0	normalization coefficient (Eq. 1.1)
x, x_0, x_1, x_2	channels aspect ratio L/D
Z, Z_0, Z_1, Z_2	channels impedance (Pa m^{-3} s)
Z_c	capillary impedance (Pa m^{-3} s)
Z_T	global impedance (Pa m^{-3} s)

Greek Symbols

$\beta, \beta_0, \beta_1, \beta_2$	channels distensibility coefficient (Pa^{-1})
γ	parameter (Eq. 4.11a)
ΔP	pressure drop (Pa)
ΔP_c	capillary hydrostatic pressure drop (Pa)
ΔP_{ci}	hydrostatic pressure drop between capillary and interstitial space (Eq.4.1) (Pa)
$\Delta \Pi_{ci}$	oncotic pressure drop (Pa)
$\Delta \Phi$	generic potential difference (Eq. 1.2)
η	dynamic viscosity (Pa s)
θ	parameter (Eq. 2.22)
λ	Lagrange multiplier
ν	kinematic viscosity (m^2 s^{-1})
f	heart-rate (s^{-1})
ξ	asymmetry factor
Π_c	capillary oncotic pressure (Pa)
Π_i	interstitial space oncotic pressure (Pa)

ρ	density (kg m^{-3})
σ_{ci}	reflection coefficient from the capillary side (page 72) (Pa^{-1} m^3 s^{-1})
σ_{ic}	reflection coefficient from the interstitial space side (page 73)(Pa^{-1} m^3 s^{-1})
τ	characteristic time (s)
ϕ	parameter (Eq. 2.28)
χ	parameter (page 40)
ω	radial angular frequency (rad s^{-1})
$\hat{\omega}$	characteristic radial angular frequency (rad s^{-1})

List of Papers

This thesis includes the following papers:

I. Carla Silva, A. Heitor Reis, ”Scaling relations of branching pulsatile flows”, International Journal of Thermal Sciences, 88, 77-83 (2015).

II. Carla Silva, A. Heitor Reis, ”Structure and adaptation of arteries to pulsatile flow: The case of the ascending aorta”, Medical Physics, 41 (6) 063701 (2014).

III. Carla Silva, A. Heitor Reis, ”Heart rate, arterial distensibility, and optimal performance of the arterial tree”, Journal of Biomechanics, 47, 2878–2882 (2014).

List of Figures

List of Tables

CHAPTER 1

Introduction

1.1 Circulatory system as a physical system

The circulatory system consists of a complex network of vessels, organized in a vascular tree, that distribute and drain blood from the different organs and tissues, in order to ensure their respective functions, and maintaining an adequate environment in tissues fluid for optimal survival and function of the cells.

The circulatory system includes the heart that pumps the blood that circulates in a network of vessels covering the entire body allowing for systemic and pulmonary circulations (see Fig 1.1). Its main function is deliver oxygen and nutrients required to sustain metabolism throughout the body and to transport the associated wasted products away. It has to continuously supply blood flow and simultaneously adjust it accordingly to the various demands of the different parts of the organism.

Blood is the fluid that transports the products related to metabolism. It is a complex heterogeneous suspension of blood cells, salts and coloids in liquid plasma, whose physical properties will be developed in §1.5. For more details please see [1].

Heart acts as a pump that creates the pressure gradient necessary to drive blood within vessels. In each contraction it supplies the required energy to maintain blood flow through all tissues in the body. Heart's left part receives oxygenated blood from the lungs, and pumps it through peripheral organs (systemic circulation), while the right part receives the blood with the wasted products of metabolism and pumps it through the lungs (pulmonary circulation). Heart ensures the connection between systemic and the pulmonary circulations of the cardiovascular system.

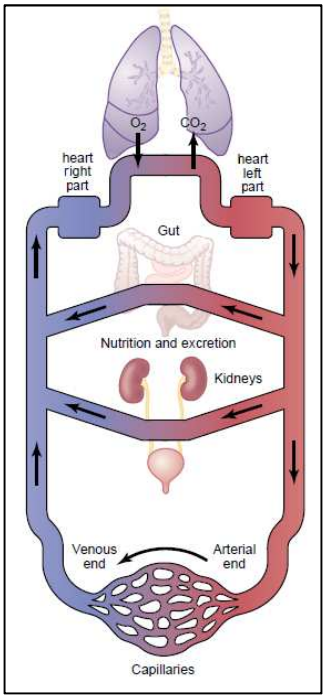

Fig. 1.1 Simplified scheme representing the organization of the circulatory system (adapted from [1]).

1.1.1 Cardiac cycle

The network of blood vessels consists of large arteries, smaller arteries, arterioles, capillaries, venules and veins (Fig. 1.2).

Aorta, the largest artery in human body, receives blood under high pressure from the heart's left ventricle, and delivers it to various part of the organism. Arteries branch into arterioles, which are the last small branches of the arterial system and have the ability to regulate the blood flow through capillaries, accordingly to the needs of the tissues.

It is at the capillary level, that oxygen and nutrients diffuse from the blood into the organs and muscles. As a consequence, blood becomes rich in wasted products (carbon dioxide, urea, creatinine); venules collect it from capillaries, merging gradually together to form veins.

In the last stage of the systemic circulation, the vena cava transports the deoxygenated blood through the heart's right ventricle, which in turn pumps it into the lungs – pulmonary circulation. Then, at the alveoli, oxygen is exchanged with the carbon dioxide. Blood returns to the left part of the heart, restarting a new cycle. In this mechanism blood passes by both circulations.

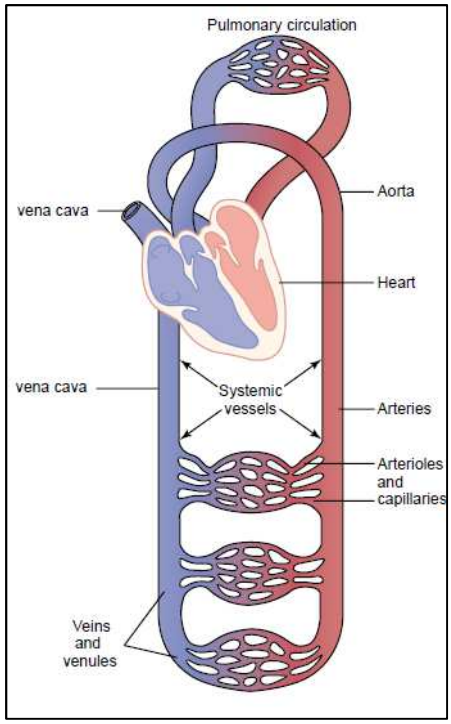

Fig. 1.2 Simplified scheme representing the organization of blood vessels in the circulatory system (adapted from [1]).

Cardiac cycle consists then of two phases: the diastole and the systole. During diastole ventricles fill in with blood, while during systole ventricles contract and pump blood out of the heart.

1.1.2 Vessels physiology

Systemic arteries are composed of large arteries, smaller arteries and arterioles. They have a thick wall divided into three concentric layers: the tunicas intima (internal layer), media and adventitia (external layer) [2]. These layers are characterized by their predominant structure and cell types (for more detailed information please see chapter 4 of ref [2]).

Arteries can be subdivided into three groups according to their elastic behavior: elastic, muscular (there are arteries that are intermediate between both types) and arterioles. Elastic arteries, which are the major distributing vessels, have relatively large diameters and are located close to the heart, such as the aorta, the common carotids or the subclavian arteries [3]. They have strong, highly elastic vascular walls, allowing for high velocity blood flow.

Muscular arteries, which comprise the main distributing branches of the arterial tree, are located at the periphery (except in the case of coronary arteries), such as radial or femoral arteries, and are characterized by less elastic walls [2].

Arteriole's walls are almost rigid and are muscular strong, having the ability of varying blood flow through the variation of the cross-sectional are, accordingly to the different demands of the tissues [1,4].

Arteries' distensible nature is a fundamental characteristic because it provides the accommodation of heart's pulsatile cardiac output in systole. The increase in vessel cross section allows for the storage of elastic energy, and consequently a creation of a forward negative pressure gradient, needed to keep blood flow during the diastole.

All along the arterial network, the distensibility of arteries is gradually reduced, leading to a drop in blood pressure. The damping in pulse pressure results then in a smooth continuous blood flow through the arteriolar level.

In contrast to the arteries, capillaries contain no muscle. Their walls are rigid and very thin, having numerous capillary pores permeable to the substances related to metabolism [1,4].

Venous system acts as a reservoir of blood. Because pressure is too low, veins' walls are thin, but muscular enough to contract or expand, acting as an adjustable reservoir according to the needs of the circulation [1-4].

To conclude this brief introduction, and to make the bridge to the next section, it is important to emphasize that the entire network in the circulatory system is composed of millions of vessels segments with different lengths and diameters, what puts at stake the question that many for long try to answer: *is the design of the vascular tree and the way vessels randomly organized, or instead is the result of some kind of optimization that obeys to a physiological or a physical principle, and in such a case calls for quantitative laws to describe the vascular structure?*

1.2 Scaling laws

Hereafter, a brief resume is presented that fits these organizations in nature, both from the biological and physiological points of view.

Life is probably the physical system that exhibit more complexity and variety on Earth. It involves more than 27 orders of magnitude, with the metabolic power required to sustain life across that range, covering over 21 orders of magnitude. The variety of forms, processes, and dynamical behaviours found in all living scales, are the result of chemical substances and chemical reactions, common to all living organisms. The processes of synthesis and degradation of nutrients in cells are due to these reactions (cellular metabolism) that are the basis of life, once it allows the growth, maintenance and reproduction of cells, ensuring their structures and adapting to environment [5,6].

In contrast to the variety and complexity of living organisms, is the probably unexpected simplicity of scaling behavior related to fundamental biological processes and covering a wide range of phenomena, and body masses, as well. Scaling laws are the reflection of generic characteristics and physical principles which are independent of specific dynamics or special characteristics of particular systems.

In biology, the observed scaling law obeys to a typically power law of the form [5-8]:

$$Y = Y_0 M^b, \tag{1.1}$$

where Y_0 is a normalization coefficient, M is body mass (independent variable), Y is some observable biological parameter and b represents the allometric scaling exponent. This exponent is verified to be approximately a multiple of ¼. Of the parameters that obey to this scaling law, among others are, metabolic rate, heart rate, growth rate, life span, lengths of aortas, tree height [9-11].

Kleiber (1930) had an important role in the study of basal metabolic rate [12], recoiling data of organisms extending in mass over about four orders of magnitude, concluding in his work that it scales as $M^{¾}$ for mammals and birds. Since then Kleiber's Law has been extended to a variety of organisms [7,13].

In order to provide a physical support to the biological empirical laws, the physicist West and the biologists Brown and Enquist, created a model that aims to explain the origin of allometric scaling laws [14]. This model was based in three assumptions: (i) a branching pattern is required along the network, in order to supply the distribution of nutrients through all tissues in the organism; (ii) the size of the smallest element of the network is fixed; (iii) minimization of energy is required in the mechanism of resources

distribution. They argued that “scaling laws arise from the interplay between physical and geometric constraints implicit in these three principles”. The concept of optimizing the pumping power for fluid flow (minimizing resistance to flow) carried out in this model, applied in circulatory and pulmonary systems of mammals resulted in the Kleiber’s Law empirical relation.

Other models have been purposed, based on physical principles namely minimal generation of entropy, maximal generation of entropy, minimization of flow resistance, the three assumptions of West, Brown and Enquist model [15].

1.3 Constructal Theory

1.3.1 Constructal Law

A year before the presentation of West, Bryan and Enquist model, a new theory has been purposed by Adrian Bejan, called Constructal Theory that in its earlier stage was applied to engineering [16].

Interesting here is that for the first time engineers participate in a discussion until then taken between physicists, biologists, zoologists and mathematicians, with a completely different point of view. Bejan says that the basis of his theory has origin in the attempt to solve a problem related to the minimization of thermal resistance between an entire heat generating volume and one point [10]. He found as the optimal solution “a tree network in which every single feature was a result, not an assumption”. He extended his conclusions to every natural (animate and inanimate) tree structure (eg. river basins, lungs, atmospheric circulation) assuming that they are the result of optimization of performance of volume-point flow. This theory somehow suggests that generation of flow configuration in nature (design in nature) is a manifestation of a universal physical phenomenon covered by a principle – Constructal Law – which states that “For a finite-size flow system to persist in time (to live) it must evolve such that it provides greater and greater access to the currents that flow through it” [10]. This means that evolution of the configuration of flow systems is predictable resulting of the way they find to improve their function, distribute imperfections and create geometries, evolving in time to minimum global flow resistance [10]. It is a kind of evolutionary principle based on the increase of flow access in time.

In nature it is not easy to find perfect geometric forms in animate systems. This means that they are far from equilibrium because they are alive. Their physical asymmetry (eg. quasicylindrical channels, quasispherical alveolus) and geometrical asymmetry (unequal distribution of stresses, temperature, pressure), i.e. their imperfections are the proof that they are alive (non-equilibrium) [17]. Despite this, these systems perform well by minimizing and balancing together the resistances found by internal and external streams under the existing global constraints. Therefore the flow system has to be free to morph, i.e. to change its configuration. The evolution of flow architecture is the result of the way that system found to achieve its global purpose under constraints.

The Constructal Law may be useful in two distinct areas: 1) to predict and explain flow configurations in animate and inanimate systems found in nature [see Fig. 1.3(b)-(e)]; 2) to be applied as a physical principle in engineering as a way of creating other architectures [see Fig. 1.3(a)].

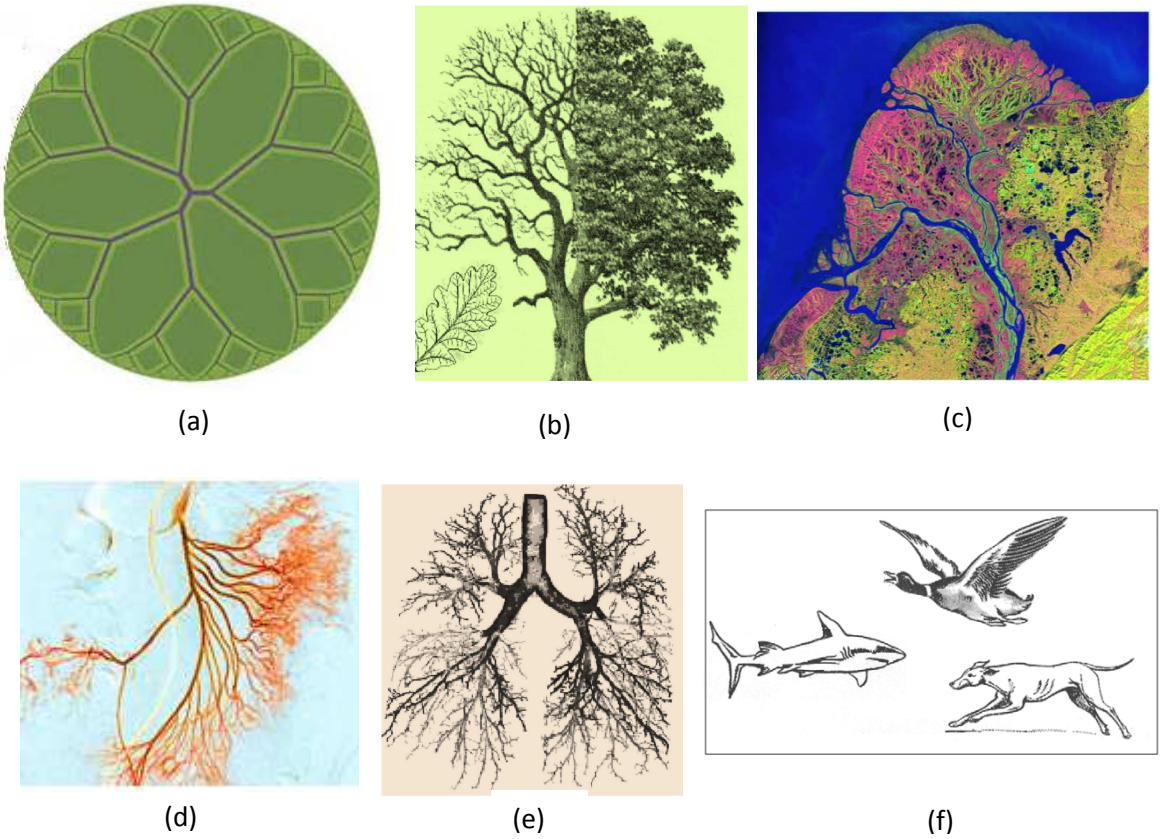

Fig. 1.3 (a) dendritic architecture derived from the constructal law. Generation of flow configuration observed in nature: (b) Vegetation – from [17]; (c) Yukon delta (inanimate flow)- adapted from USGS site; (d) blood vessels - adapted from Science Photo Lib; (e) bronchial tree – from [17]; (f) animal locomotion (flying, running and swimming) - adapted from [21].

The constructal theory, based on the principle of evolution of configuration generation for greater flow access in time, successfully anticipates the 23-level bifurcation (Fig. 1.3c) of the lung [18], the scaling laws of all river basins [19] and macroscopic features (speed, frequencies, forces) of all types of animal locomotion (running, swimming, flying) [20].

Constructal theory has also been considered in the conception of a model of the long-term behavior of the atmospheric and oceanic circulation (climate), the largest flow system on Earth. For a detailed analysis of the model and results please see [17,22].

This theory has also been considered in an interesting work [23] who aims to describe and predict the formation of different patterns within elements of the same species under distinct hydrodynamics conditions. The study covered stony corals, bacterial colonies and plant roots. Other applications of constructal law to animate and inanimate nature flows and more complete information may be found in refs [10,17,24].

Man-made flow systems (engineering) evolves similarly and are predictable based on the same principle that explains the evolution and architecture of natural flow systems. The increase of heat transfer in systems is one of the most active applications of constructal theory in engineering. A lot of industrial devices, as air conditioners, refrigeration systems, radiators, use a kind of tubes (fined or non-fined) arrangement as heat exchangers. In the design of these heat exchangers some features as the space available in the equipment must be considered. From the constructal theory point of view, the basis of the formulation of the problem is identifying the configuration which provides maximum heat transfer in a confined space.
Other applications of engineering flow configurations with more complete information may be found in refs [10,17,24,25].

1.3.2 Constructal Theory and Thermodynamics

Constructal Law states that if a flow system has freedom to change its configuration, it will show different configurations in time, in order to provide gradually better access routes to the flowing currents. Constructal theory is then assumed as an extension of thermodynamics [26] in the domain of non-equilibrium systems with flow

configuration. Actually let us take the example of an isolated thermodynamic system which has within a partition that suddenly breaks; in the beginning the system is in a state of internal non-uniformity - different parts are submitted to different pressure or temperature. According to the two laws of thermodynamics, this system tends to a state of equilibrium with: 1) no flows of matter or energy; 2) maximum entropy; 3) constant energy. In equilibrium there are no driving forces. Flow configurations in time are unknown. From the thermodynamic point of view the system is a black box. Constructal theory intends to cover the phenomenon of systems' flow configurations evolution in time, before reaching the state of equilibrium.

Open systems, like biological systems, are permanently in a non-equilibrium state. They are continuously exchanging energy and mass with the environment. Classical thermodynamics does not take in account flow configurations of non-equilibrium systems. From the constructal point of view, currents are organized in order to provide gradually better access routes between inlet and outlet flow currents, making it by minimizing global flow resistance. Bejan and Lorente demonstrated in ref [27] that non-equilibrium flow systems evolve in time toward an equilibrium configuration. They argued that "Equilibrium does not mean that the flow architecture stops changing. On the contrary, it is here at equilibrium that the flow geometry enjoys most freedom to change".

Thermodynamics studies equilibrium states whereas Constructal Theory studies the evolution of flow configurations towards the equilibrium. Equilibrium states arise from second law whereas equilibrium flow configurations arise from constructal law. This formal analogy between thermodynamics and constructal theory, concerning aspects as their concepts, statements and principles are described in Table 1.1.

Further we can relate entropy generation to constructal law; we note that the common feature shared by flows in nature and engineered systems is that they are both dissipative. These flows generally can be described as:

$$R = \frac{\Delta\Phi}{I}, \tag{1.2}$$

where R is the resistance to flow and $\Delta\Phi$ corresponds to the potential driving the current I. These flows generate entropy at the rate $\dot{S}_{gen} = \Delta\Phi\, I / T$, where T is thermodynamic temperature. The resistance can be expressed as

$$R = \frac{\dot{S}_{gen}\, \mathrm{T}}{I^2}. \tag{1.3}$$

We can associate the maximization of internal flow access to the minimization of flow resistance. The analysis of Eq. (1.3) allows one to conclude that, at constant I, minimizing flow resistance corresponds to minimizing the entropy generation rate. Conversely, if we fix the forces ($\Delta\Phi$) minimizing the resistance corresponds to maximizing the entropy generation rate [28].

In conclusion we can associate generation of entropy to the Second Law, and generation of flow architecture to Constructal Law [17].

Table 1.1 Analogy between the concepts, statements, and principles of thermodynamics and constructal theory [27].

Thermodynamics	**Constructal Theory**
State	Flow architecture (geometry, structure)
Process	Change of structure
Properties (U, S, Vol, ….)	Global objective and global constraints (R, L, V,…)
Equilibrium state	Equilibrium flow architecture
Fundamental relation U (S, Vol, …)	Fundamental relation R (L, V,…)
Constrained equilibrium states	Nonequilibrium architectures
Removal of constraints	Increased freedom to morph
Energy minimum principle: U minimum at constant S and Vol S maximum at constant U and Vol	Constructal principle (maximization of flow access): R minimum at constant L and V V minimum at constant R and L L maximum at constant V and R

To complete §1.3 it should be noted that Constructal Law covers the three postulates of West et al. model [14]. Constructal theory is able to explain a broad diversity of flow architectures found in nature [21] – river basins, animal locomotion, turbulence – that stay out of the domain covered by West et al. model. Murray's Law (see §1.4), a scaling law applied to dichotomous branching is also consequence of the application of Constructal Law to engineered systems [29].

Constructal Theory can be naturally assumed as a unifying principle that introduces the concept of "designedness" in nature not covered by first physical principles, and reveals be able to explain animate and inanimate flow configurations. Applied progress made based on this theory, with emphasis on the last decade may be found in ref [30].

1.4 Murray's Law

A special class of scaling laws was studied by Murray. In 1926, he proposed a principle of minimum energy dissipation to explain the relation between diameters (father and daughter channels) in dichotomous branching.

He assumed that the quantitative statement which includes the physiologic organization concept is a principle that states "that the cost of operation of physiological systems tends to be a minimum" [31-33]. Based on the principle of minimum work and balanced cooperation of the organs in the body, Murray's law states that "the cube of the radius (or equivalently the diameters) of a parent vessel equals the sum of the cubes of the radii of the daughters", applied to bifurcation channels with non-turbulent flows:

$$D_0^3 = D_1^3 + D_2^3 \tag{1.4}$$

where D_0 is parent vessel diameter and D_1 e D_2 stands for the diameters of daughter vessels (Fig. 1.4).

This law was firstly applied to circulatory and respiratory system, but later studies show that it holds for every branching laminar flow [10,29,33].

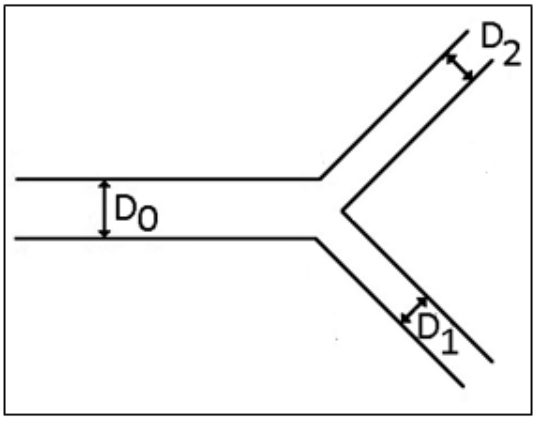

Fig. 1.4 Representation of a dichotomous branching.

Based on Constructal theory and considering Murray Law, Reis et al. [18] have successfully anticipated the verified 23-level bifurcation of the lungs. Also Wechsatol et al. [34] used Murray Law to find the optimal tree-shaped networks for fluid flow in a disc-shaped body, related to components of electronic cooling.

This scaling law is also a consequence of Constructal Law [21].

1.5 Blood flow characteristics

As seen before, in the circulatory system blood transports nutrients through the body tissues and then removes the associated waste products. It has to flow through a complex vascular network, in which diameters vary from approximately 3 cm in the aorta, down to about 6 μm at the capillary level.

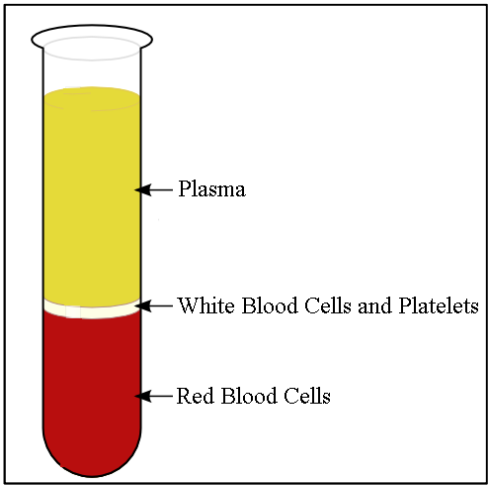

Fig. 1.5 Centrifuged Blood Sample (adapted from Wikipédia).

A flow rate has to be kept in circulation in order to guarantee the organism necessities. This rate strongly depends on, among others, the flow properties of the blood and its constituent characteristics.

Blood is a suspension of plasma and cells. Plasma is a dilute electrolyte solution that makes up about 55% of whole blood volume in a normal human body; it contains minerals, glucose, proteins, hormones and carbon dioxide. Plasma serves as a protein reserve of human body. The remaining 45% are occupied by blood cells such as red blood cells (RBC - nearly 95% of whole cells), white blood cells (WBC - less than 0.15%) and platelets (5%) (see Fig. 1.5) [2].

Red blood cells are dominant making up 40% by volume of whole blood. White blood cells and platelets occupy less than 1%.

The high concentration of red blood cells is very important from the rheological point of view, especially due to the properties of these cells [35]. They are small semisolid particles, which are highly deformable [36]. At rest, red blood cells look like biconcave disks with a mean diameter of about 8.5 μm and a thickness of 2.5 μm (see Fig. 1.6) at the thickest point and about 1.0 μm or less in the center [1].

They can pass through capillaries of diameter 5.0 μm, due to the flexibility of their membrane.

1.5.1 Blood rheology

Blood rheological properties are determined by its constituents. Blood viscosity depends on existing shear forces and is a function of: 1) hematocrit (volume percentage of RBC in blood); 2) plasma viscosity; 3) RBC aggregation and 4) RBC mechanical properties [37].

As a consequence of experimental data (see Fig 1.7), it was found that, in healthy conditions, bloods exhibits shear-thinning behavior, i.e. blood viscosity decreases to a minimum value with increasing shear rates, while it is higher at low shear rates [38,39].

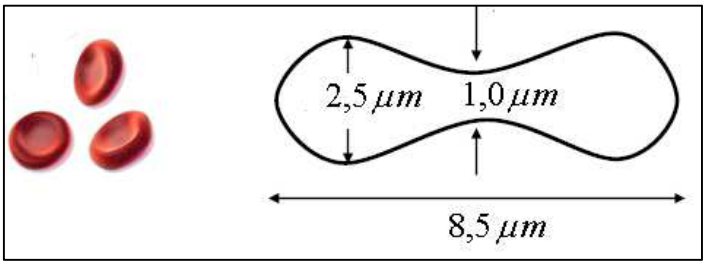

Fig. 1.6 Shape of Red Blood Cells at rest (adapted from Wikipédia).

Blood behaves as a Newtonian fluid at high shear rates above 100 s^{-1}, with viscosity of about 4 to 5 Pa.s $\times 10^{-3}$, at a normal hematocrit of 45% at 37 ^{o}C [37,40]. At shear-rates below 100 s^{-1}, blood viscosity increases exponentially with decreasing shear rate (see Fig 1.7) [38].

Blood viscosity behavior is explained based on RBC properties. They are highly deformable and therefore might change their shape under shear forces, in order to adapt to flow conditions (bulk flow or microcirculation); they squeeze through capillaries, having the ability to deform in almost any shape [1, 2].

Another property of normal RBCs is their particular tendency to aggregate in rouleaux (linear arrays) disposed like stacks of coins [2,35,41], behaving like a solid. The size of these aggregates is inversely proportional to shear forces having a strong influence in the definition of blood viscosity.

So, at higher shear-rate these aggregates tends to break down and RBCs orient in the direction of the flow and consequently viscosity is lower. On the other hand, at low shear-rate and under low flow or almost static conditions, there is a trend of RBCs to aggregate, resulting in the disturbance of blood flow streamlines, increasing viscosity to higher values [1,2,35].

Some studies concluded another blood property related to the reduction of its apparent viscosity as the tube diameter becomes smaller [42]. Farhaeus and Lindqvist performed experiments with blood at high shear rates and verified that apparent viscosity is lower in small tubes when compared to larger tubes [41,43].

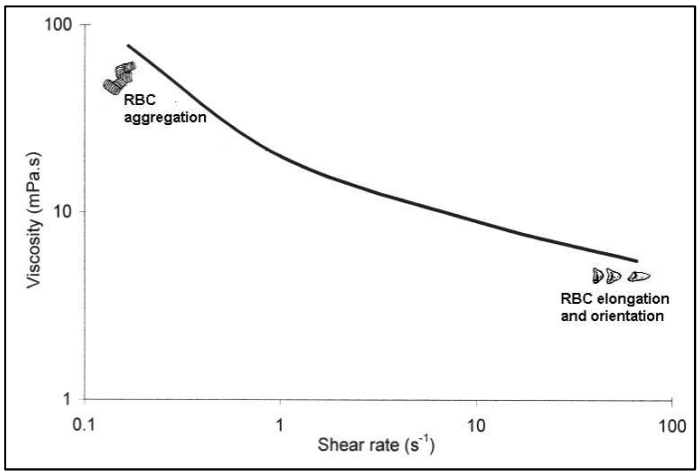

Fig. 1.7 Blood viscosity as a function of shear rate (adapted from [35]).

This reduction in blood viscosity with decreasing vessel diameter reaches a minimum value around 6 to 8 μm; as the diameter becomes even smaller viscosity increases abruptly (see Fig 1.8) [42,44]. This is called Fahraeus-Lindqvist effect, and has its physical reason based on the formation of a cell-free layer near the tube wall, so that RBCs move along the central region, resulting in the decrease of flow resistance [35,41,45].

Actually, since red blood cells are small semisolid particles, they affect the viscosity and the behavior of the fluid. Blood viscosity is not constant at all flow rates and exhibits mostly non-newtonian behavior at the microcirculatory level.

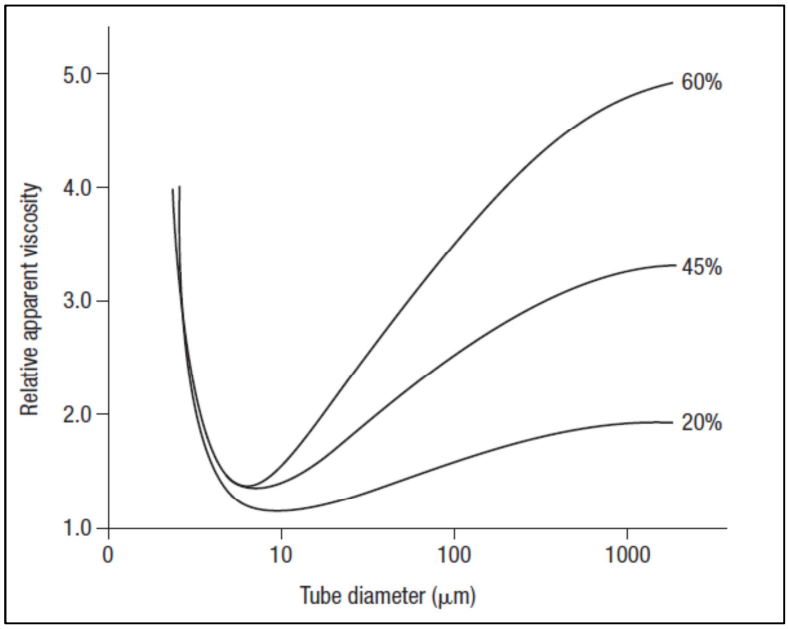

Fig. 1.8 Variation of relative apparent viscosity with diameter in microvessel, showing Fahraeus-Lindqvist effect, for different values of hemathocrit (adapted from [2]).

However, in most arteries, where diameter is large compared to the RBCs size (diameter exceeding 1 mm), blood is usually exposed to high shear-rates (above $100s^{-1}$) and hence the non-Newtonian effects which are relevant at low shear-rates, disappear [46,47]. This condition, therefore excludes arterioles, venules, and capillaries, once they are generally considerably less than 1 mm in diameter. In tubes with diameter less than 1 mm, blood viscosity is dependent on shear-rate [2].

It is clear that blood viscosity depends on shear-rate. Since the most available information includes data of blood viscosity as a function of shear-rate, and our modeling of the arterial tree (§3) requires the assignment of a viscosity to each vessel diameter, we adopt the values in table 1.2 based on data in ref [48]. On our work we assign a shear-rate to a diameter and so a diameter to a viscosity.

Table 1.2 was drawn on the basis of an estimate, that introduces little inaccuracy but which doesn't affect directly the final conclusions, once that with our work we intend to analyse trends of the circulatory system, not to obtain accurate values.

1.5.2 Reynolds number

The Reynolds number (R_e) is used in order to predict the flow regime (laminar or turbulent) that is associated with blood flow in arteries, through the expression:

$$R_e = \frac{\rho u D}{\eta} \ . \tag{1.5}$$

In healthy conditions, we can calculate R_e, associated with a large artery, by considering the order of the values involved: blood density $\rho \sim 10^3 kg\ m^{-3}$, blood average velocity $u \sim 10^{-1} ms^{-1}$, vessel diameter $D \sim 10^{-2} m$, and blood dynamic viscosity $\eta \sim 10^{-3} Pa\ s$. Therefore, Reynolds number is of order $R_e \sim 10^3$.

Table 1.2 Range of blood viscosity values and respective diameter vessel.

Diameter (mm)	**Blood Viscosity (Pa.s×10^{-3})**
> 10	4 – 6
5 – 10	6 – 9
< 5	9 – 15

This result enables us to assume that in normal conditions blood flow in large arteries is typically laminar. Downstream in arterial tree, flow regime remains laminar as can be verified through Eq. (1.5). Actually, Reynolds number varies proportionally to *D* and *u*, which both decrease as arteries become smaller. Furthermore blood viscosity increases, resulting in a Reynolds number smaller than 10^3, therefore ensuring a laminar flow regime at almost arteries in healthy conditions.

1.5.3 Hagen-Poiseuille Equation

For simplicity we consider Navier-Stokes equation applied to a unidirectional blood flow:

$$\frac{\partial u}{\partial t} + u \,.\, \text{grad u} = -\frac{1}{\rho}\,\text{grad P} + \nu\, lap\ \text{u}\ . \tag{1.6}$$

We conclude that for the case of pulsatile blood flow in humans, the terms *∂u/∂t* and $u.grad\ u$ are about one and two orders of magnitude smaller, respectively, than the remaining terms in Eq. (1.6). Therefore, at a first approximation their contribution may be discarded. For detailed discussion of this point please see §3.2.

Blood flow is then determined by: (i) the pressure gradient developed in the vessel (driving force); (ii) the friction force (brake) developed in the flow within the vessel.

From the previous analysis, we may consider the simplest model of steady laminar flow i.e. the Hagen-Poiseuille equation applied to an axisymmetric flow in a circular tube (vessel) of diameter *D* and length *L* that reads:

$$I = k_A^{-1}\frac{D^4}{L}\Delta P\,, \tag{1.7}$$

where *I* is the flow rate, $k_A = 128\mu/\pi$ is a constant, μ is dynamic viscosity and ΔP is pressure gradient along the vessel.

Making an analogy to Ohm's Law $I = \Delta P / R$, one concludes from Eq. (1.7) that the resistance to flow is

$$R = k_A \frac{L}{D^4}\,. \tag{1.8}$$

We can verify that blood flow resistance increases with dynamic viscosity and decreases with diameter fourth-power. Clogging of an artery resulting in decrease of diameter leads to enormous increase in flow resistance, with bad consequences to the performance of the circulatory system.

1.6 Models of the circulatory system

In this section we aim to give a brief description of some models that have been developed to simulate blood flow in the cardiovascular system, and also their advantages and disadvantages. As reviewed in §1.1, the cardiovascular system consists of heart, systemic and pulmonary circulations (blood vessels), and has associated nervous and biochemical regulators which may alter vessel parameters (eg. distensibility, vessel diameter) as a way of regulating the variables of the system (pressure blood, flow rate), according to the needs of organism different parts (organs). The study and conception of cardiovascular models is an important tool, which reveals to be helpful in the understanding of the complex interactions and physiological functions permanently occurring in the human body [1].

Over time many models of the cardiovascular system have been developed [2,49] to study either single arteries or the circulatory of specific organs.

These models are usually described by a set of mathematical equations relating some of the variables of the system, which in turn are dependent of the parameters of the system, as blood viscosity, vessel dimensions, distensibility, which are almost impossible to measure.

The arterial system may be modelled by means of lumped models [50,51], distributed models [52,53] and tube models [54].

1.6.1 Lumped models (Windkessel model)

The Windkessel model is the most popular lumped parameter or simplified model. When applied to arterial system it has several applications [49,56,57], namely as a way to understand some functions of the cardiovascular system, to predict some arterial parameters and to derive aortic flow from arterial pressure.

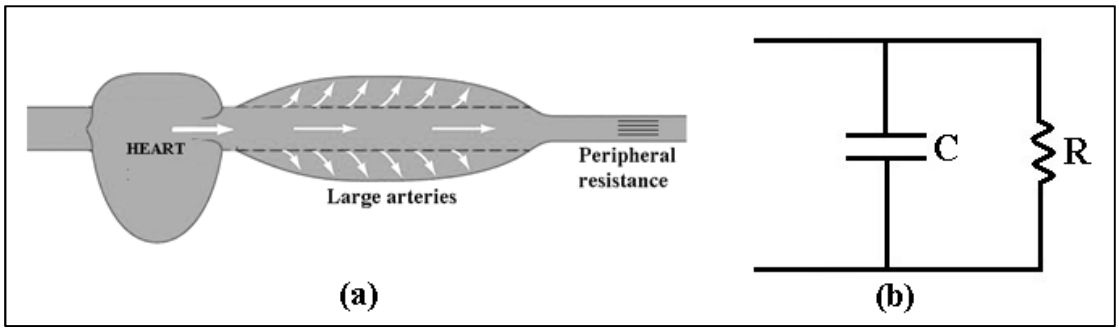

Fig. 1.9 Representation of two-element Windkessel model for the arterial system. (a) Conception: peripheral resistance is the sum of the resistances of small arteries, arterioles and capillaries; large arteries (remarkably the aorta) represent compliant part whose total compliance is the sum of the arteries' compliance [55]; (b) Electrical analog.

These kind of lumped models describe the whole arterial system as a function pressure - flow rate, staying out of this analysis the phenomena that occur within the arterial system, such as wave travel or reflection of waves [55], see Fig. 1.9.

This model has successfully anticipated some results related to aortic pressure in function of time [55], see Fig. 1.10. More specifically it was found that in the diastole (when the aortic valve is closed) pressure decays exponentially with a characteristic time decay ($\tau = RC$). He succeed to derive cardiac output and to estimate the total peripheral resistance [56].

This model has the disadvantage of neglecting either the resistance of large arteries either the compliance of the smaller vessels, introducing a rough approximation. It fails to explain the pressure abruptly variation during systole [55].

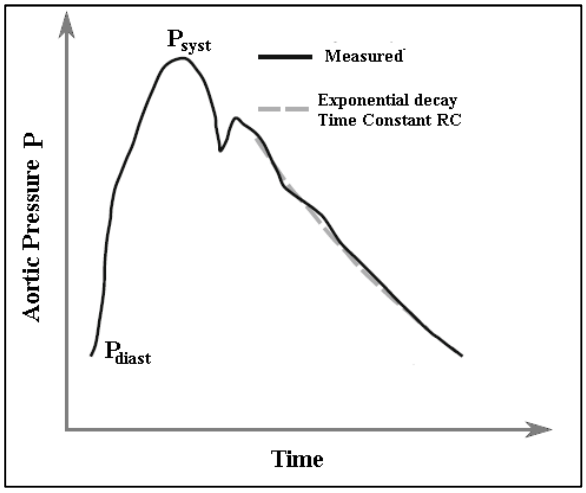

Fig. 1.10 Aortic pressure during a heart period

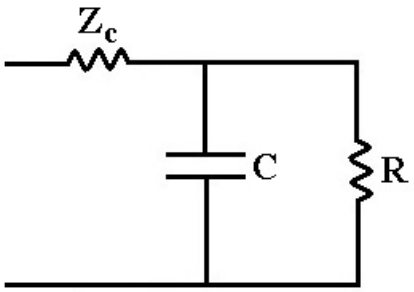

Fig. 1.11 Electrical representation of three-element Windkessel model.

A few years later (in the 1930s), and as a way to improve the two-element model, some researchers proposed the consideration of a third element, the characteristic impedance of the aorta (Z_c). This new term takes in account the local inertia and local compliance of the proximal ascending aorta, on the bases of wave transmission theory (for more detailed information please see [56]).

Z_c is connected in series as represented in Fig. 1.11, where is showed an electrical analog of three-element Windkessel model.

The consideration of the third element improves the behavior of the model in the range of high frequencies [2,56]. This lumped model is very popular and is often considerate in the modeling of the systemic circulation.

The proposal of introducing a fourth element to this model [58], was intended as a way of reducing some errors introduced by the characteristic impedance at low frequencies. An inertial term (*L*) was introduced in parallel with the characteristic impedance (see Fig. 1.12).

This element represents the sum of the inertances associated to the arterial segments. Thus, total inertance and total compliance of the arterial system, corresponds to each arterial segment, while in the previous model the characteristic impedance was only associated to proximal ascending aorta [55]. Westerhof et al. [58] concluded that this model was better than the three-element, as a lumped model of the systemic circulation or as a model to estimate vascular properties.

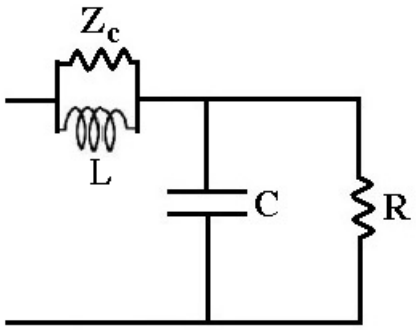

Fig. 1.12 Electrical representation of fourth-element Windkessel model.

1.6.2 Distributed models and tube models

Windkessel models give a general description of the arterial tree as a whole, therefore not allowing the study of pressure or flow wave propagation along the vascular tree. Modelling the phenomena of wave propagation in the arterial system requires the use of tube models or distributed models [56].

Distributed models account to the detailed vascular geometry. Basis of these models is formed by breaking up the arterial tree into several segments (see Fig. 1.13) of known geometry and mechanical properties [59]. The description of the wave transmission characteristics related to each arterial segment, may be described using Womersley oscillatory flow theory or electrical transmission line theory (for more detailed information please see [59] and chapter 8 of [56]). These models can also be based on the Navier-Stokes equations for the conservation of mass and momentum, in one-dimension form, written as a function of pressure, blood flow and cross sectional area, and can be solved by using different numerical techniques [56].

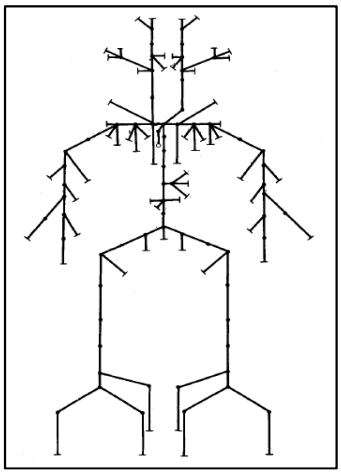

Fig. 1.13 Representation of the human arterial tree. Each segment represents an artery (adapted from [60]).

These models provide good descriptions of the arterial system, for the reason that they consider the geometry of each vessel and the general anatomy. Distributed models enable the study of aortic impedance and the factor determining it [59]. They also allow the understanding of pressures and flows in different parts of the organism [56]. These models have the disadvantage of requiring a wide number of parameters related to geometry and elasticity of each segment, becoming a little limited.

Another kind of model which reveals to be simple and with the advantage of considering the phenomena of wave propagation, is the single tube and the asymmetric T-tube models [56, 60]. They prove to be much easier to translate into a code when compared to the geometrically exact models [59].

Single tube models consider the combination of a tube representing the aorta connected to a peripheral resistance or Windkessel (as a model of the peripheral beds). The simplicity of this model has its main drawback when considering that all distal reflections came from a single point [56].

On the other hand, asymmetric T-tube models seem to better describe the arterial tree in terms of aortic input impedance and wave reflections [56]. They consist of two parallel tubes: a short one accounting the arterial tree related to head and arms, and a long one with larger size representing the thoracic and abdominal aorta and their branches including the legs [56]. The two tubes terminate either with a resistance of the terminal bed.

The choice of the model depends on whether is the detailed required or its main purpose. Distributed models are commonly used as analytical tools once they are realistic in the simulation of a wide of physiological and pathological situations. They allow the estimation of parameters of arterial tree based on *in vivo* data [61]. Lumped models are adopted namely to understand the influence of total arterial compliance on integrated quantities, as aortic pressure or cardiac output [55].

In next section it is presented our modelling of the circulatory system, as well as its main features and the purpose of its application.

1.7 Modelling of the circulatory system used in this thesis

The definition of our model of the circulatory system is based on Constructal Theory. Constructal method consists of optimization of the system at every scale, i.e. by optimizing performance by vessel to vessel we reach optimization of the overall system. As stated by constructal law, the method proceeds from the simple to the complex, so the starting point is the optimization of the element and then, step by step, towards optimization of the global system.

Our modelling consists of representing each vessel by a RC model. Although some models of the circulatory system referred at §1.5.3 are based on RC models, our purpose is quite different once we intend to optimize the arterial tree by starting from each element (vessel). In almost available models the resistance or capacitance values results of some kind of vessel network, which is distinct from ours in which each single artery is represented by a RC model.

As stated in §1.1, blood vessels are generally more or less distensible, which reveals to be an important property. Actually, due to the high resistance to flow observed in microcirculation (blood flow in capillaries and the interstitial space) a relatively high perfusion pressure is required for the transport of blood, that can be achieved only if the vessels' walls are elastic therefore avoiding heart´s overloading due to pumping [61,63].

Blood flow in the arterial tree is markedly pulsatile. The cardiac cycle, represented in Fig. 1.14, consists of two distinct parts: 1) systole corresponding to blood pumping out of the heart, while ventricles contract; 2) diastole during which ventricles fill with blood.

The distension of the arterial wall during the propagation of the peak of the pressure wave, thereby increasing the cross section of the vessel and lowering the resistance, also allows storage of elastic energy, which makes it possible the maintenance of a negative pressure gradient along the vessel, needed to keep the flow in the diastole.

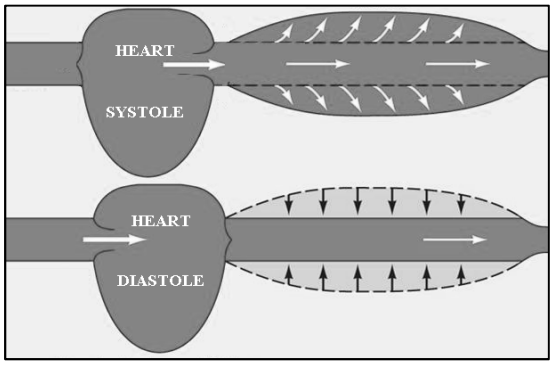

Fig. 1.14 Representation of the effect of the systole and diastole in vessel distensibility.

Then, vessel distensibility is a relevant parameter in the formulation of our model. In this way we define the capacitance of storage or vascular capacitance C as the linear relationship between volume variation and pressure variation, i.e.

$$C = \frac{dV}{dP} \tag{1.9}$$

We further define the distensibility coefficient $\beta = A^{-1}\left(dA/dP\right)$, where *A* stands for the channel cross sectional area.

Considering a cylindrical vessel of diameter *D* and length *L*, the respective volume is $V = \pi D^2 L / 4$. The capacitance or compliance may be expressed as $C = (\pi / 2) DL\left(\partial D/\partial P\right)$

By simplifying the expression, we can write $\beta = \left(2/D\right)\left(\partial D/\partial P\right)$. Then the compliance of the vessel [Eq. (1.9)] can be expressed as a function of distensibility coefficient β as:

$$C = k_B D^2 L, \tag{1.10}$$

where k_B is a constant ($k_B = \pi\beta / 4$).

Because it combines the effect of the usual resistance with the capacitive effect of the vessel walls, we found that an equivalent parallel RC circuit, Fig. 1.15, is the most suitable model for describing pulsating flow.

Following the discussion in §1.5.3, we identify the value of resistance with that of Poiseuille flow [Eq. (1.8)] while the capacitance part is defined by Eq. (1.10). In the representation of Fig. 1.15 the capacitor discharge corresponds to the artery elastic recoil that “pushes” the flow at diastole.

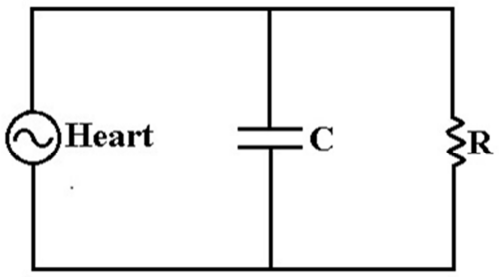

Fig. 1.15 Representation of an RC circuit simulating a vessel.

The RC circuit total impedance *Z* is given by,

$$\frac{1}{Z}=\frac{1}{R}+\frac{1}{X_c}, \tag{1.11}$$

where R is resistance to flow and $X_c = 1/(i\omega C)$ is capacitive reactance (*C* is capacitance and ω angular pulse frequency).

Therefore Eq. (1.11) reads,

$$\frac{1}{Z}=\frac{1}{R}+i\omega C\ . \tag{1.12}$$

The modulus of the impedance is then,

$$|Z|=\frac{R}{\sqrt{1+\omega^2R^2C^2}}, \tag{1.13}$$

where $R=k_A L\, D^{-4}$, $C=k_B D^2 L$ with $k_A=128\mu/\pi$ and $k_B=\pi\beta/4$.

Though *D* is a function of time, here it stands for the average of *D* over a cycle.

This model will be applied to the human arterial tree to enable the study of the arteries' behavior under pulsatile flow.

1.8 Outline of the thesis

This thesis is composed of five chapters, and includes three papers that have been submitted to scientific journals. Chapter 1 is a general introduction to the thesis, where concepts and theories related to the circulatory system, blood rheology, Constructal Theory and some cardiovascular system models, are briefly presented.

Chapter 2 presents the development of a model of a pulsatile flow system aiming at finding the respective scaling laws viewed as extensions of Murray's Law for continuous flow. Each channel in the system network is represented as a resistive-

capacitive model (RC), and its resistance to flow is approached in terms of a mean impedance (impedance modulus). Hereafter, we define the total impedance modulus to flow of a dichotomous branching of cylindrical channels. Based on Constructal theory, the global impedance of the channels that converge in a bifurcation is minimized under constant global volume of the flow tree, and then with the additional condition of minimization under constant pressure head. The main objective is to define the optimal scaling laws of diameters and lengths of branching cylindrical channels, and to interpret the results both by comparing with Murray's law, and by analysing the effects of distensibility on the optimal performance of the system.

In chapter 3 the previous developed model will be applied specifically to the human arterial tree with the aim of understanding the behaviour of some arteries in different aspects, namely their impedance during lifetime and the influence of heart rate on impedance. In the light of the developed model, it will be also carried out the study of some arterial segments, namely to investigate if its structure is optimized relatively to blood flow, and then comparing the results with observed data. Finally an interpretation of the verified lifelong elongation of the ascending aorta is presented. The whole study is carried out with data of healthy subjects.

Chapter 4 presents an explanation to the observed reduction of arterial distensibility with heart rate, in the radial and carotid arteries, based on the model developed in chapter 2. The main purpose is actually to explore once again the applicability of this model to the human arterial tree, by using observed physiological data found in literature.

Chapter 5 presents the general conclusions of the work developed in this thesis.

In the end of each chapter of this thesis the respective bibliography is presented.

References

[1] A. C. Guyton, and J. E. Hall, *Textbook of Medical Physiology*, 11th ed., Elsevier Saunders, Pennsylvania (2006).

[2] W. W. Nichols, M. F. O'Rourke, C. Vlachopoulos, *McDonald's Blood Flow in Arteries Theoretical - Experimental and Clinical Principles*, 6th ed., Hodder Arnold, London (2011).

[3] Lauralee Sherwood, *Fundamentals of Human Physiology*, 4th ed., Brooks/Cole, Cengage Learning (2012).

[4] J. R. Levick, *An Introduction to Cardiovascular Physiology*, 2nd ed, Butterworth-Heinemann Ltd., Oxford (1995).

[5] G. B. West, "The Origin of Universal Scaling Laws in Biology", *Physica A,* 263: 104 – 113 (1999).

[6] K. Schmidt-Nielsen, *Scaling: Why is Animal Size so Important*, Cambridge University Press, Cambridge, (1984), 7-29.

[7] K. J. Niklas, *Plant Allometry: The Scaling of Form and Process*, Univ. of Chicago Press, (1994), chapter 1.

[8] V. M. Savage, J. F. Gilooly, W. H. Woodruff, G. B. West, A. P. Allen, B. J. Enquist and J. H. Brown, "The predominance of quarter-power scaling in biology", *Functional Ecology,* 18: 257–282 (2004).

[9] G.B. West, J. H. Brown, "Life's universal scaling laws", *Physics Today,* 36–42 (2004).

[10] A. Bejan, *Shape and Structure, from Engineering to Nature*, Cambridge University Press, (2000).

[11] G. B. West, W.H. Woodruff, J.H. Brown, "Allometric scaling of metabolism from molecules and mitochondria to cells and mammals", *Proc. Nat. Ac. Sci. U. S. A.,* 99: 2473-2478 (2002).

[12] Max Kleiber, "Body size and metabolism", *Hilgardia* 6: 315–353 (1932).

[13] John Prothero, "Scaling of energy metabolism in unicellular organisms: a re-analysis", *Comp. Biochem. Physiol.,* 83A (2), 243-248 (1986).

[14] G.B. West, J. H. Brown, B. J. Enquist, "A general model for the origin of allometric scaling laws in biology", *Science*, 276: 122–126 (1997).

[15] A. Bejan, S. Lorente, "The constructal law of design and evolution in nature", *Phil. Trans. R. Soc. B,* 365: 1335–1347 (2010).

[16] A. Bejan, "Constructal-theory network of conducting paths for cooling a heat generating volume", *Int. J. Heat Mass Transfer,* 40: 799–816 (1997).

[17] A. H. Reis, "Constructal Theory: From Engineering to Physics, and How Flow Systems Develop Shape and Structure", *Appl. Mech. Rev*, 59: 269-282 (2006).

[18] A. H. Reis, A. F. Miguel, M. Aydin, "Constructal theory of flow architecture of the lungs", *Medical Physics*, 31: 1135–1140 (2004).

[19] A. H. Reis, “Constructal view of scaling laws of river basins”, *Geomorphology* 78: 201–206 (2006).

[20] A. Bejan, J. H. Marden, “Unifying constructal theory for scale effects in running, swimming and flying”, *Journal Theoretical Biology,* 209: 238–248 (2006).

[21] A. Bejan, J. H. Marden, “The constructal unification of biological and geophysical design”, *Physics of Life Reviews*, 6: 85-102 (2009).

[22] A. H. Reis, A. Bejan, “Constructal theory of global circulation and climate”, *Int. J. of Heat and Mass Transfer*, 49: 1857–1875 (2006).

[23] A. F. Miguel, “Constructal pattern formation in stony corals, bacterial colonies and plant roots under different hydrodynamics conditions”, *Journal of Theoretical Biology*, 242: 954-961 (2006).

[24] A. Bejan and S. Lorente, *Design with Constructal Theory*, Wiley Hoboken (2008).

[25] A. Bejan, S. Lorente, “Constructal theory of generation of configuration in nature and engineering”, *Journal of Applied Physics,* 100: 041301-1 - 041301-23 (2006).

[26] A. Bejan, *Advanced Engineering Thermodynamics*, 2nd ed. Wiley, New York (1997).

[27] A. Bejan, S. Lorente, “The constructal law and the thermodynamics of flow systems with configuration”, *Int. J. of Heat and Mass Transfer*, 47: 3203–3214 (2004).

[28] A. H. Reis, “Use and validity of principles of extremum of entropy production in the study of complex systems”, *Annals of Physics*, 346: 22-27 (2014).

[29] A. Bejan, L. A. O. Rocha, S. Lorente, T- and Y-shaped constructs of fluid streams, *International Journal of Thermal Sciences*, 39: 949–960 (2000).

[30] A. Bejan and S. Lorente, “Constructal law of design and evolution: Physics, biology, technology, and society”, *J. Appl. Phys*., 113, 151301 (2013).

[31] C. D. Murray, “The Physiological Principle of Minimum Work. I. The vascular system and the cost of blood volume”, *Proc. Nat. Ac. Sci. U. S. A.,* 12 (3): 207–214 (1926).

[32] C. D. Murray, “The Physiological Principle of Minimum Work. II. Oxygen exchange in capillaries”, *Proc. Nat. Ac. Sci. U. S. A.,* 12 (5): 299–304 (1926).

[33] T. F. Sherman, “On connecting large vessels to small: The meaning of Murray's Law”, *The Journal of General Physiology,* 78 (4): 431–453 (1981).

[34] W. Wechsatol, S. Lorente, A. Bejan, “Optimal Tree-Shaped Net- works for Fluid Flow in a Disc-Shaped Body”, *Int. J. of Heat and Mass Transfer*, 45(25): 4911–4924 (2002).

[35] O. K. Baskurt, M. R. Hardeman, M. W. Rampling, *Handbook of Hemorheology and Hemodynamics*, IOS Press, Netherlands (2007).

[36] Kim Youngchan, Kim Kyoohyun, YongKeun Park, "Measurement Techniques for Red Blood Cell Deformability: Recent Advances, Blood Cell - An Overview of Studies in Hematology", dx.doi.org/10.5772/50698 (2012).

[37] O. K. Baskurt, H. J. Meiselman, Blood Rheology and Hemodynamics, Seminars in Thrombosis and Hemostasis, 29(5): 435-450 (2003).

[38] E. W. Merrill, "Rheology of blood", *Physiological Reviews*, 49: 863–888 (1969).

[39] P. W. Rand, E. Lacombe, H. E. Hunt, W. H. Austin, "Viscosity of normal human blood under normothermic and hypothermic conditions", *J Appl Physiol,* 19: 117–122 (1964).

[40] David Elad and Shmuel Einav, *Standard Handbook of biomedical engineering and design*, McGraw-Hill, chapter 3 (2004).

[41] C. G. Caro, T. J. Pedley, R. C. Schroter and W. A. Seed, *The mechanics of the circulation*, 2nd ed., Cambridge University Press (2012).

[42] H. L. Goldsmith, G. Cokelet, P. Gaehtgens, "Robin Fahraeus: evolution of his concepts in cardiovascular physiology", *Am. J. Physiol*., 257: H1005-H1015 (1989).

[43] R. Fahraeus, T. Lindqvist, "The viscosity of blood in narrow capillary tubes", *Am J Physiol.*, 96: 562–568 (1931).

[44] A. A Stadler, E. P. Zilow, O. Linderkamp, "Blood viscosity and optimal hematocrit in narrow tubes", *Biorheology* 27(5): 779–788 (1990).

[45] O. K. Baskurt, H. J. Meiselman, "Hemodynamic effects of red blood cell aggregation", *Indian Journal of Experimental Biology*, 45: 25-31 (2007).

[46] K. Perktold, G. Karner, A. Leuprecht and M. Hofer, "Influence of Non-newtonian Flow Behavior on Local Hemodynamics", *ZAMM - Journal of Applied Mathematics and Mechanics*, 79: 187-190 (1999).

[47] D. N. Ku, "Blood flow in arteries", *Annual Reviews of Fluid Mechanics,* 29: 399-434 (1997).

[48] B. Canaud, I. Jaussent, A. Rodriguez, H. Leray-Moragues, L. Chenine, A. Picard, M. Morena, J. P. Cristol, "Whole-blood viscosity increases significantly in small arteries and capillaries in hemodiafiltration. Does acute hemorheological change trigger cardiovascular risk events in hemodialysis patient?", *Hemodialysis International*, 14: 433–440 (2010).

[49] Joseph D. Bronzino, *The Biomedical Engineering Handbook*, 3rd ed., Trinity College Hartford, Connecticut, chapter 10 (2006).

[50] M. R. Mirzaee, O. Ghasemalizadeh, B. Firoozabadi, “Simulating of Human Cardiovascular System and Blood Vessel Obstruction Using Lumped Method”, World Academy of Science, Engineering and Technology 41 (2008).

[51] M. S. Olufsen, A. Nadim, “On deriving lumped models for blood flow and pressure in the systemic arteries”, *Mathematical Biosciences and Engineering*, 1 (1): 61-80 (2004).

[52] P. Reymond, F. Merenda, F. Perren, D. Rüfenacht, N. Stergiopulos, “Validation of a one-dimensional model of the systemic arterial tree”, *Am. J. Physiol. Heart Circ. Physiol.,* 297: H208–H222 (2009).

[53] H. F. O’Rourke, A. P. Avolio, “Pulsatile flow and pressure in human systemic arteries: studies in man and in a multi-branched model of the human systemic arterial tree”, *Circulation Research*, 46: 363–372 (1980).

[54] D. S. Berger, J. K-J Li, A. Noordergraaf, “Arterial wave propagation phenomena ventricular work and power dissipation”, *Ann. Biomed. Eng*., 23: 804-811 (1995).

[55] N. Westerhof, J. W. Lankhaar, B. E. Westerhof, “The arterial Windkessel”, *Medical and Biological Engineering and Computing*, 47: 131–141, (2009).

[56] N. Westerhof, N. Stergiopulos, M. I. M. Noble, *Snapshots of Hemodynamics - An Aid for Clinical Research and Graduate Education*, 2nd ed., Springer, London (2010).

[57] E. B. Shim, J. Y. Sah, C. H. Youn, “Mathematical modelling of cardiovascular system dynamics using a lumped parameter method”, *Japanese Journal of Physiology*, 54: 545-553 (2004).

[58] N. Stergiopulos, B. E. Westerhof, N. Westerhof, “Total arterial inertance as the fourth element of the windkessel model”, *American Physiological Society* (1999).

[59] J. T. Ottesen, M. Danielsen, *Mathematical Modelling in Medicine*, IOS Press, Amsterdam, 65-78 (2000).

[60] M. G. Taylor, “Wave transmission through an assembly of randomly branching elastic tubes”, *Biophysics Journal,* 6: 697–716 (1966).

[61] A. P. Avolio, “Multi-branched model of the human arterial system”, *Medical & Biological Engineering & Computing*, 18: 709-718 (1980).

[62] K. M. Taylor, W. H. Bain, K. G. Davidson, M. A. Turner, “Comparative clinical study of pulsatile and non-pulsatile perfusion in 350 consecutive patients”, *Thorax* 37, 324-330 (1982).

[63] C. Mavroudis, “To pulse or not to pulse”, *The Annals Thor. Surg.*, 25: 259-271 (1978).

CHAPTER 2

Scaling relations of branching pulsatile flows*

Abstract

Apparently complex flow structures obey to scaling laws that enable to make it viable the study of their configuration and flow dynamics. This is the case of flow structures that exhibit several branching levels and are thought to perform optimally.

Here we present the scaling laws of diameters and lengths of branching cylindrical channels with pulsatile flows, and compare them with other relations published in the literature. It is shown that, under constant global volume of the flow tree, and for zero pulse frequency these scaling laws reduce to Murrays's law of consecutive diameters. Optimal scaling depends on pulse frequency, distensibility of the channel walls, and asymmetry of the daughter vessels. In case that in addition to global volume of the flow tree, the pressure head is also kept constant, a similar scaling law of channel lengths emerges that holds together with the law of diameter scaling. The effect of channel distensibility is shown to be somehow important, such that for achieving optimal performance (lowest impedance) channels with lower relative distensibility must have their diameter increased. Results are compared with those of other models for the case of some arteries.

Keywords: branching flows, scaling, Murray's law, pulsatile flow, Constructal theory.

*Carla Silva, A. Heitor Reis, "Scaling relations of branching pulsatile flows", International Journal of Thermal Sciences, 88, 77-83 (2015).

2.1 Introduction

Murray's Law [1-3] which states that the "cube of the radius of a parent vessel equals the sum of the cubes of the radii of the daughters" stays as a landmark scaling law of geometries of branching channels with non-turbulent flows (see Fig. 2.1). It was originally proposed by Cecil D. Murray (1926) for the circulatory and respiratory systems, yet later on has been proved to hold for every branching laminar flow [3,4].

Murray stated in his original work [2] that physiologic organization should be based on principle and pointed out minimum work and balanced cooperation of the organs in the body as the best candidate for such a principle. Sherman [3] provided a full derivation of Murray's law based on that principle. Allometric scaling laws are common in biology and, with the purpose of their explanation, approaches have been developed based on optimal performance of the whole system, either through minimization of energy dissipation [5] or through flow configuration that enables maximum flow access [6]. West and co-workers [5] presented a general model of allometric scaling relations (WBE model) in that the ratio between the diameters of consecutive arteries, D_{k+1}/D_k, is $n^{-1/2}$ for arteries, and $n^{-1/3}$ for small vessels (n stands for branching ratio), regardless of the length of the vessels.

Murray's Law has also been considered in the context of engineered systems. About a decade ago, Bejan and coworkers [4] proved that Murray's law may be deduced from a general principle - the Constructal Law (1997) – which states: "For a finite-size system to persist in time (to live), it must evolve in such a way that it provides easier access to the imposed currents that flow through it." (see for instance ref. [7]). Said another way, Constructal Law entails evolution of flow architecture in such a way that under the existing constraints the distribution of flow resistances evolves in time to achieve minimum global flow resistance.

Under the conjecture that Nature has optimized in time the living structures, Reis and coworkers [8] applied both Murray's Law and Constructal Law to successfully anticipate some architectural features of the lung tree. More complete information about the successful application of the Constructal Law may be found in Bejan [6], Reis [9], and Bejan and Lorente [10].

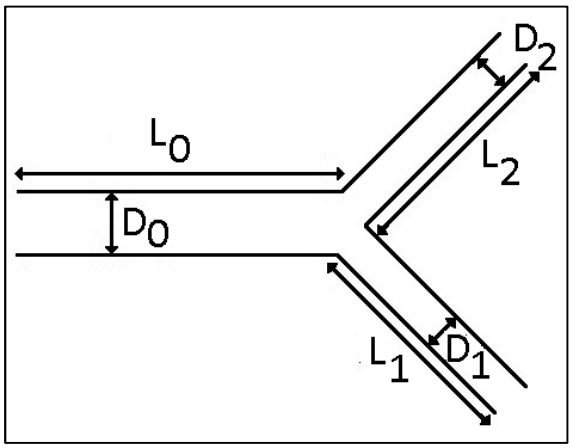

Fig. 2.1 Branching channels with distensible walls (D – diameter; L – length).

However, we note that with respect to optimal performance Mauroy et al. [11] have put forward the idea that "the optimal system is dangerously sensitive to fluctuations or physiological variability, such that physical optimality cannot be the only criterion for design".

With respect to optimal scaling in asymmetric branching, Bejan [7] has shown that

$$\frac{D_1}{D_0}=\left(1+\xi^3\right)^{-1/3},\quad \frac{D_1}{D_2}=\frac{L_1}{L_2}, \tag{2.1}$$

where $D_2/D_1=L_2/L_1=\xi$, is the asymmetry factor of daughter vessels, and the subscripts 0, 1, 2 represent the parent and each one of the daughter vessels, respectively. The Eq. (2.1) which relates homothety coefficient with asymmetry factor further adds to the study of scaling in asymmetric flows, which are shown to be important for achieving optimal performance of flow trees [12].

In the following we will further extend this analysis to find out the scaling relations of branching pulsatile flows.

2.2 Pulsatile flows

Flows that develop in circulatory trees are ubiquitous in Nature. In some animals, namely the vertebrates, blood is rhythmically pumped through the entire body at a broad range of pulse rates. It is recognized that pulsatile flow performs best than continuous flow because it induces lower overall resistances [13] and also better blood perfusion [14].

The most complete model of pulsatile flows, was put forward by Womersley [15] who solved Navier-Stokes equation in channel with elastic walls and periodic pressure forcing, and provided formulas for the pressure wave, and the radial and longitudinal components of the velocity field in the arteries. This work that stays as a landmark in the field was used as one of the basis of the WBE model [5].

Since then, other works have appeared that modelled pulsating flows in rigid channels [16]. Noteworthy are those of Nield and Kuznetzov [17], Siegel and Perlmutter [18] and Faghri et al. [19], albeit these studies were also carried out under the "rigid channel" assumption. Models using analogy with electric circuits date back to about several years ago. Remarkable by its complexity are those of Tsitlik et al. [20], Avolio [21], or recently that of Mirzaee et al. [22].

With the purpose of optimizing branching structures with pulsatile flows, in what follows we will further explore the parallel RC model. Though Womersley's equations describe pulsatile flows accurately, they are quite complex, and not easy to handle analytically in the study of branching vessels. This is why we use an RC model as a suitable description of pulsatile flow. In this model the flow induced by the pressure wave "charges the capacitor" (the arterial elastic walls) while it is braked by a "Poiseuille resistance" in the flow direction. The rationale for using Poiseuille flow, rather than considering a more complex model based on the Navier-Stokes equation is explained in the following.

Let us start from Navier-Stokes equation for unidirectional flow: $\partial u/\partial t + u.grad\ u = -\rho^{-1} grad\ P + \nu\, lap\ u$. In the case of pulsatile flow in arteries, the inertial terms may be discarded because they are, at least, of one order of magnitude smaller than the other terms, as it is shown through scale analysis. In this way, let u denote average blood velocity, τ characteristic time related to pulse wave frequency, L_c the characteristic length in the flow direction, D vessel diameter, ρ blood density, ΔP pressure variation along the vessel and ν blood kinematic viscosity. Then, by assuming the following scale values for large arteries: $u \sim 10^{-1} ms^{-1}$, $\tau \sim 1s$, $L_c \sim 1m$, $D \sim 10^{-3} m$, $\Delta P \sim 10^{3} Pa$ and $\nu \sim 10^{-5} m^2 s^{-1}$, the orders of magnitude (in ms^{-2}) of the terms in the Navier-Stokes equation are: $\partial u/\partial t \sim 10^{-1}$, $u.gradu \sim 10^{-2}$, $\rho^{-1} gradP \sim 1$,

$vlap\ u \sim 1$, therefore justifying the use of Poiseuille flow as a first approach in the study of the human arterial system. Models that include the term $\partial u/\partial t$ lead to greater complexity in the calculations but did not cause a change in the conclusions. For example, the RLC model developed by Jager and co-workers [23] accounts for the "sleeve effect", which arises from the interaction between viscous and inertial terms in the Navier-Stokes equation. However, in the same study [23] it was shown that the "sleeve effect" is important in some arteries at frequencies higher than 15 rad s^{-1}, which is somehow beyond the normal range of the human pulse frequency.

In real systems, pressure waves of some frequency travel all along the circulatory trees. Energy in circulatory trees travels in the form of enthalpy plus mechanical energy of the bulk fluid, and in the form of elastic energy of the vessel walls.

As the basis for building up a model of a pulsatile flow driven by a pressure difference ΔP in a vessel of length L and diameter D, one starts from the Hagen-Poiseuille equation in the form:

$$I = k_A^{-1} L^{-1} D^4 \Delta P, \tag{2.2}$$

where *I* is current ($m^3\ s^{-1}$), $k_A = 128\mu/\pi$, in which μ is dynamic viscosity of the fluid. In pulsatile flow, both ΔP and *D* are functions of time, and therefore the same happens with the conductance $K_p = k_A^{-1} L^{-1} D^4$. In what follows the variables D, L, V standing for geometric features of vessels with pulsatile flow represent values averaged over a cycle. In this way, as a first approximation we will consider the actual conductance in the channel as the sum of the average conductance (corresponding to diameter *D*) plus the deviation corresponding to diameter variation with pressure, i.e.

$$K_p(t) = K + \overline{K}' = k_A^{-1} L^{-1} D^4 \left(1 + 2\beta \left(dP/dt\right)_0 \Delta t\right), \tag{2.3}$$

where $\beta = \left(2/D\right)\left(\partial D/\partial P\right)$ is the distensibility coefficient and Δt is the time elapsed after the channel diameter has reached the average value. The Eq. (2.3) shows that the conductance is the sum of two terms: the first one corresponds to the inverse of the usual resistance while the second one is equivalent to the inverse of a capacitive

resistance. This aspect is made clearer if we consider $I(t)=K_p(t)\Delta P(t)$ together with Eq. (2.3) to obtain:

$$I \approx k_A^{-1}L^{-1}D^4\Delta P + 2k_A^{-1}L^{-1}D^4(\Delta t)\beta\Delta P\left(dP/dt\right)_0. \tag{2.4}$$

Eq. (2.4) shows that the flow in a channel with elastic walls is composed of two terms: one corresponds to a resistive current,

$$I_r = k_A^{-1}L^{-1}D^4\Delta P, \tag{2.5}$$

while the other matches up a capacitive current,

$$I_c = 2I_r(\Delta t)\beta\left(dP/dt\right)_0, \tag{2.6}$$

with capacitance $C = 2I_r(\Delta t)\beta$, (see Fig.2.2).

As the global conductance is the sum of the respective conductances, one concludes that an equivalent parallel RC circuit is the model suitable for describing pulsatile flow (see Fig.2.3).

2.3 Minimization of impedance in branching pulsatile flows

As pressure increases in the channel, the elastic walls are strained to accommodate more fluid. The capacitance *C*, which has the same meaning as compliance in vessel physiology, is defined as $C = dV/dP$. For a cylindrical channel, with volume $V = \pi D^2 L/4$, one obtains:

$$C = k_B D^2 L, \tag{2.7}$$

with $k_B = \pi\beta/4$.

Fig. 2.2 Channel wall distensibility is accounted for by an analog to electric capacitance, while flow resistance is that of Hagen-Poiseuille flow.

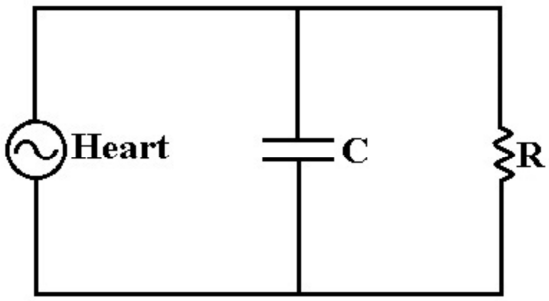

Fig. 2.3 Pulsatile flow as an analogue to a parallel RC circuit.

The Eq. (2.7) provides the opportunity for conferring some significance to Δt in Eq. (2.6). Then, by putting together $C = 2I_r(\Delta t)\beta$ and $C = k_B D^2 L$ we get $C = (\pi D^2 L / 8)/I_r$. Therefore, Δt would stand for the time required for the averaged current I_r to fill half of the channel volume. However, we note that Eq. (2.3) was put forward simply with the purpose of justifying the existence a capacitive flow, together with a resistive flow in the case of a deformable channel, and will not be used in what follows.

Additionally, the resistance is given by [see Eq. (2.5)]:

$$R = k_A L D^{-4}. \tag{2.8}$$

Let us consider a channel with elastic walls with a pressure wave of frequency ω. By analogy with the electric circuit model (Fig. 2.3), the total impedance *Z* of such channel reads:

$$|Z| = R\left(1 + \omega^2 R^2 C^2\right)^{-1/2}, \tag{2.9}$$

which with Eqs. (2.7) and (2.8) and $x = L/D$, $y = D^3$, $k = k_A k_B$ becomes:

$$|Z| = k_A x y^{-1}\left(1 + \omega^2 k^2 x^4\right)^{-1/2}, \quad kx^2 = 1/\hat{\omega} \tag{2.10}$$

where $\hat{\omega}$ represents the characteristic frequency of the channel.

2.3.1 Minimization of global impedance under constant volume

Now, let us consider a channel that branches in two different channels, as represented in Fig. 2.1. For the vast majority of flow systems in the conditions described above (Eqs.(3.7) and (3.8)) we have (see Appendix).

$$|Z|_T = |Z|_0 + \left(|Z|_1^{-1} + |Z|_2^{-1}\right)^{-1}. \tag{2.11}$$

By taking into account Eq. (2.10), the Eq. (2.11) reads:

$$|Z|_T = \frac{k_A x_0 y_0^{-1}}{\left(1+\omega^2 k_0^2 x_0^4\right)^{1/2}} + \left(\frac{\left(1+\omega^2 k_1^2 x_1^4\right)^{1/2}}{k_A x_1 y_1^{-1}} + \frac{\left(1+\omega^2 k_2^2 x_2^4\right)^{1/2}}{k_A x_2 y_2^{-1}} \right)^{-1} . \tag{2.12}$$

The volume of a cylindrical vessel is $V = (\pi/4)D^2 L$. With $\tilde{V} = 4V/\pi$, the total volume $\tilde{V}_T$ occupied by the flow system is,

$$\tilde{V}_T = D_0^2 L_0 + D_1^2 L_1 + D_2^2 L_2 = x_0 y_0 + x_1 y_1 + x_2 y_2 \ . \tag{2.13}$$

In Eqs. (2.12) and (2.13) *x* and *y* are free variables that describe the branching structure. The condition of easiest flow access is achieved with the minimization of the global flow impedance under constant global volume of the channels, $\tilde{V}_T$,

$$d|Z|_T - \lambda d\tilde{V}_T = 0 , \tag{2.14}$$

where λ is a constant.

We chose the aspect ratios {x_0, x_1, x_2} as design variables subject to optimization for the reason that $x = L/D$ defines channel geometry better than either *D* or *L* alone.

By minimizing the global impedance $|Z|_T$ [Eq. (2.12)] under constant volume with respect to each of design variables {x_0, x_1, x_2} one obtains, respectively:

$$\lambda = \frac{k_A}{y_0^2}\left(A_0^{-1/2} - 2\omega^2 k_0^2 x_0^4 A_0^{-3/2}\right), \tag{2.15}$$

$$\lambda = \frac{k_A B^2}{x_1^2}\left(A_1^{1/2} - 2\omega^2 k_1^2 x_1^4 A_1^{-1/2}\right) , \tag{2.16}$$

$$\lambda = \frac{k_A B^2}{x_2^2}\left(A_2^{1/2} - 2\omega^2 k_2^2 x_2^4 A_2^{-1/2}\right) , \tag{2.17}$$

where $A_i = 1 + \omega^2 k_i^2 x_i^4$, *i = 0, 1, 2*, and $B = \left(A_1^{1/2} x_1^{-1} y_1 + A_2^{1/2} x_2^{-1} y_2\right)^{-1}$. Therefore, with the definition of A_i, and Eqs. (2.16) and (2.17) one obtains:

$$\left(A_1^{1/2} - 2A_1^{-1/2}\right)(A_1 - 1)^{-1/2} = \left(A_2^{1/2} - 2A_2^{-1/2}\right)(A_2 - 1)^{-1/2} . \tag{2.18}$$

A solution to Eq. (2.18) is,

$$A_1 = A_2 . \tag{2.19}$$

This first result, indicates that for minimal resistance to flow the characteristic frequencies $\hat{\omega}_i = 1/R_i C_i = 1/k_i x_i^2$ [see Eq. (2.10)] of the two daughter channels must be equal.

By using $A_i = 1 + \omega^2 k_i^2 x_i^4$ together with Eqs. (2.16), (2.17) and (2.19) one obtains:

$$\frac{D_1}{D_0} = \theta^{1/6}\left(1+\xi^3\right)^{-1/3}, \tag{2.20}$$

$$\frac{D_2}{D_0} = \theta^{1/6}\left(1+\xi^{-3}\right)^{-1/3}, \tag{2.21}$$

where

$$\theta = \left(2A_i^{-3/2} - A_i^{-1/2}\right) \Big/ \left(2A_0^{-3/2} - A_0^{-1/2}\right), \; i = 1, 2 \tag{2.22}$$

and $\xi = L_2 / L_1$ stands for branching asymmetry. Taking together the eqs. (2.20) and (2.21) one has,

$$D_0^3 = \theta^{-1/2}\left(D_1^3 + D_2^3\right). \tag{2.23}$$

For non-pulsatile flow ($A_i = 1$; $\theta = 1$) the Eq. (2.23) reduces to the known form of Murray's Law:

$$D_0^3 = D_1^3 + D_2^3 \ . \tag{2.24}$$

Additionally, from Eq. (2.20) and Eq. (2.21) we obtain the following relationship:

$$\frac{D_2}{D_1} = \frac{L_2}{L_1} = \xi, \tag{2.25}$$

or, in view of Eq. (2.19):

$$x_1 = x_2 \, ; \beta_1 = \beta_2 . \tag{2.26}$$

The equations (2.26) show that in optimal flow branching the daughter channels share the same aspect ratio *x* and distensibility coefficient β.

By using the Eqs. (2.19)-(2.21), and (2.26) as the results of the optimization, and $\hat{\omega}_i = 1/k_i x_i^2$, and $A_i = 1+\omega^2 k_i^2 x_i^4$, we obtain the minimal impedance from Eq. (2.12) in the form

$$|Z|_{T,opt} = \frac{4}{\pi\beta_0 L_0 D_0^2 \hat{\omega}_0 A_0^{1/2}}\left(1+\frac{L_1}{L_o}\left(1+\xi^3\right)^{1/3}\phi^{-1}\right), \tag{2.27}$$

where

$$\phi = \theta^{2/3}\left(\frac{A_1}{A_0}\right)^{1/2}. \tag{2.28}$$

Now we are able to assess the effect of pulsation on the impedance of the bifurcation represented in Fig. 2.1. By noting that non-pulsatile flow corresponds to $A_1 = A_0 = 1$ and $\theta = 1$, therefore $|Z|_T$ reduces to the usual resistance *R*, we can represent the ratio $|Z|_T/R$ as a function of frequency as shown in Fig. 2.4 for various values of $\chi = \hat{\omega}_1/\hat{\omega}_0$, and for the particular case of symmetric branching $\xi = 1$ and $L_1 = 0.5L_0$. For the same $x = L/D$, we note that $\chi < 1$ stands for a daughter channel of higher distensibility with relation to the father channel $(\beta_1/\beta_0 > 1)$, while $\chi > 1$ represents just the reverse. As shown in Fig. 2.4 the effect of pulsation becomes significant as the pulse frequency approaches the characteristic vessel frequency $\hat{\omega}_0$, namely for $\omega/\hat{\omega}_0 > 0.1$. In the case when the daughter channel is less distensible $(\chi > 1)$ pulse frequency significantly reduces flow impedance, an effect that for the same $x = L/D$ increases with the inverse of the distensibility ratio $\beta_0/\beta_1 = \hat{\omega}_1/\hat{\omega}_0 = \chi$ (see Fig. 2.4). On the contrary, in the case when the daughter channel is more distensible pulse frequency increases impedance as the pulse frequency falls in the vicinity of the characteristic parent channel frequency $\hat{\omega}_0$.

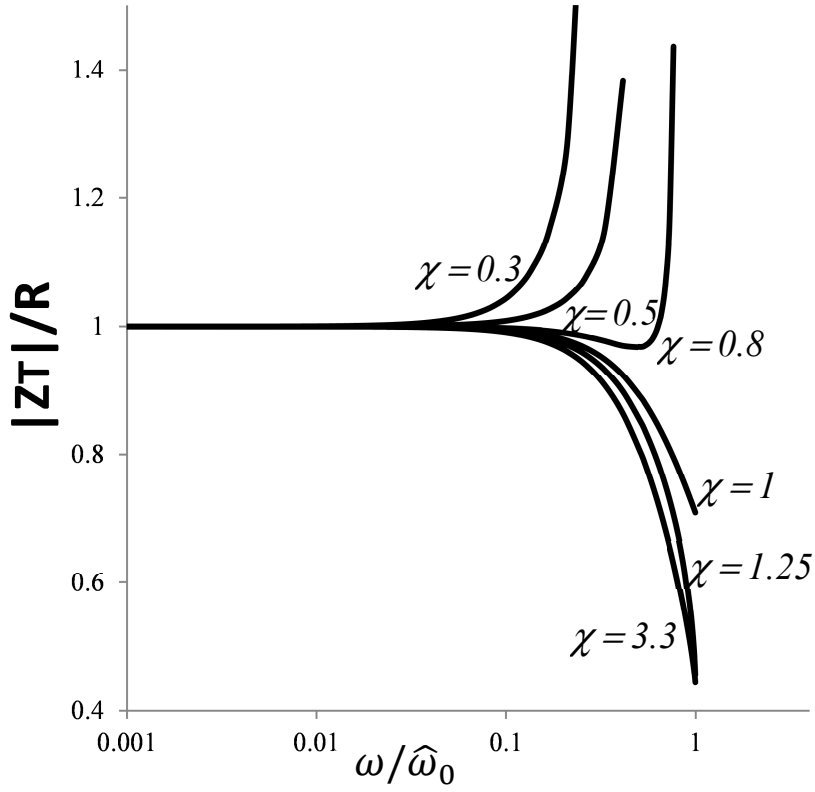

Fig. 2.4 The effect of the relative characteristic frequencies of parent ($\hat{\omega}_0$) and daughter channel ($\hat{\omega}_1$), (with $\chi = \hat{\omega}_1/\hat{\omega}_0$ =0.8, 0.5, 0.3, 1, 1.25, 3.3), on impedance as function of pulse frequency.

2.3.2 Minimization of global impedance under constant volume and pressure head

Reis [9] has shown that minimal global flow resistance in a branching tree under constant total pressure head, ΔP, is achieved with a tree configuration in which total flow resistances allocated to flow are the same at each branching level. This means that in the best performing (optimal) flow system design both the overall resistance and pressure drop distribute in such a way that their respective values do not change from a branching level to the next one. This result enables generalize the scaling laws of channel length for pulsatile flow. The Eq. (2.27) shows that the minimal impedance of the branching channel is the sum of two terms: the first one corresponds to the father channel while the second one stands for the global impedance of the branching channels. Because they must have the same value one obtains:

$$\frac{L_1}{L_o} = \phi\left(1+\xi^3\right)^{-1/3}, \tag{2.29}$$

where we used A_i as defined above. Similarly, one obtains:

$$\frac{L_2}{L_o} = \phi\left(1+\xi^{-3}\right)^{-1/3}. \tag{2.30}$$

To conclude, in case that both volume and pressure head are kept constant, the global impedance of an optimal tree with *N-1* branching levels with pulsatile flow of frequency ω reads,

$$\left|Z\right|_{T,opt} = N\frac{4}{\pi\beta_0 L_0 D_0^2 \hat{\omega}_0 A_0^{1/2}}, \tag{2.31}$$

where $\hat{\omega}_0 = \left(k_0 L_0^2 / D_0^2\right)^{-1}$ is the characteristic frequency of the parent channel.

2.3.3 Scaling of unstrained channel diameters with different distensibilities

We recall that *D* in Eqs. (2.20-2.25) refers to channel diameters averaged over a cycle. Because average channel diameter D may be expressed in terms of its unstrained value D_{us} plus a term corresponding to an average dilation, i.e. $D = D_{us}\left(1+\beta P^+/2\right)$, where $P^+ = P(D) - P(D_{us})$, the Eqs. (2.20) and (2.21) read:

$$\frac{D_{1us}}{D_{0us}} = \frac{\left(1+\beta_0 P^+/2\right)}{\left(1+\beta_1 P^+/2\right)}\theta^{1/6}\left(1+\xi^3\right)^{-1/3},\ \frac{D_{2us}}{D_{0us}} = \frac{\left(1+\beta_0 P^+/2\right)}{\left(1+\beta_2 P^+/2\right)}\theta^{1/6}\left(1+\xi^{-3}\right)^{-1/3}. \tag{2.32}$$

As a consequence the unstrained diameters ratios of parent to daughter channels will be affected as function of channel distensibilities and the pressure excursion during the pulse [see Eqs. (2.32)].

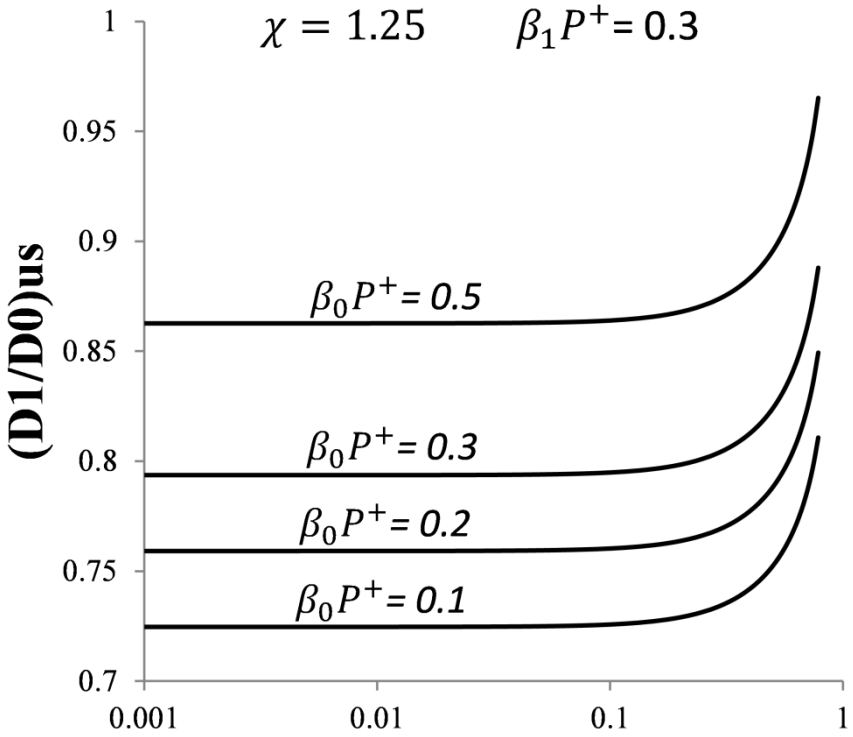

Fig. 2.5 Daughter to parent unstrained diameter ratios as function of pulse frequency for various channel distensibilities for the case when $\chi = 1.25$.

Fig. 2.5 shows the unstrained diameter ratios (D_{1us}/D_{0us}) as function of frequency for the case when $\chi = 1.25$, and for various values of $\beta_0 P^+$. With χ fixed, because $\chi = \hat{\omega}_1/\hat{\omega}_0 = (\beta_0/\beta_1)\left(x_0^2/x_1^2\right)$ [see Eqs. (2.7)-(2.10)], note that the ratio β_0/β_1 depends only upon the ratio x_0^2/x_1^2, therefore making it possible to explore both the cases when $\beta_1 > \beta_0$ and $\beta_1 < \beta_0$. We observe that for optimal performance (lowest impedance) the unstrained diameter ratios must decrease with $\beta_0 P^+$, which means that decreasing distensibility of parent channel leads to increase in its diameter. The same behavior is observed for the case when $\chi = 0.8$ (see Fig. 2.6). Specifically for $\omega/\hat{\omega}_0 > 0.1$ the unstrained diameter ratios (D_{1us}/D_{0us}) increase with pulse frequency when $\chi = 1.25$, and decrease with pulse frequency when $\chi = 0.8$.

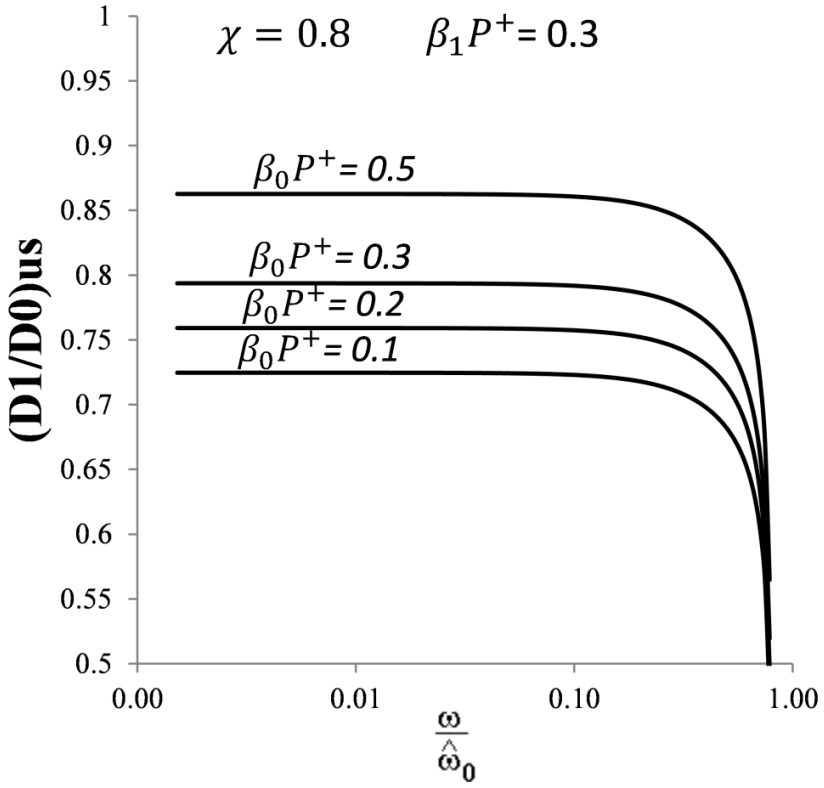

Fig. 2.6 Daughter to parent unstrained diameter ratios as function of pulse frequency for various channel distensibilities for the case when $\chi = 0.8$.

The human arterial system is an example of a tree with pulsatile flow in which the average pressure head varies in time. Therefore, optimal scaling of such a tree is described by the Eqs. (2.19)-(2.28) and (2.32).

A key aspect of scaling that match minimal impedance in branching channels with pulsatile flow, and with variable pressure head, is that scaling depends upon pulse frequency. For non-pulsatile flow ($\omega = 0, A_i = 1$) in channels with asymmetric branching the Eqs. (2.20)-(2.21) reduce to the already known scaling for continuous flow Eq. (2.1).

The Eqs. [(2.20)-(2.23)] and [(2.29)-(2.30)] represent a generalization of Murray's Law for pulsatile flow in a channel with branching asymmetry. Asymmetry of branching is accounted for the parameter $\xi = L_2 / L_1$, which through Eq. (2.20) and Eq. (2.21) assigns a smaller diameter to the shorter branch. On the other hand, the global impedance of the pulsatile flow tree depends upon the pulse frequency ω. This is a new and very

important result that will be explored in a subsequent study of the human circulatory system viewed as a flow tree with pulsatile flow.

2.3.4 Comparison of the results of the models of Murray, WBE and this model

In order to compare the predictions of the model above developed with those of other models that present scaling relations for diameters in dichotomous branching, we start from the general scaling relation:

$$\frac{D_{n+1}}{D_n} = a\,(1+\varepsilon)^{-\alpha} \tag{2.33}$$

where as a rule $\varepsilon = 1$ appears in the scaling relations of dichotomous branching, α is the scaling exponent, and a is an additional parameter. To the parameters in Eq. (2.33) Murray's law assigns the fixed values: $a = 1$, $\varepsilon = 1$ and $\alpha = 1/3$, while in the WBE model [5] $a = 1$, $\varepsilon = 1$, and $\alpha = 1/2$ for the branching levels up to a nonspecified level k, while $\alpha = 1/3$ "for large *k*, corresponding to small vessels" [5]. In the present model, $a = \theta^{1/6}$, $\varepsilon = \xi^{3}$ or $\varepsilon = \xi^{-3}$ (depending on the degree of asymmetry of daughter vessels), and $\alpha = 1/3$ (see Eqs. (2.20) and (2.21)). For the sake of comparison we further define the variable

$$\psi = \ln\left(\frac{D_{n+1}}{D_n}\right) \tag{2.34}$$

Therefore, Murray's law is represented by $\psi = -(1/3)\ln 2 = 0.231$, in the WBE model $\psi = -(1/2)\ln 2 = 0.347$, or for large branching order *k*, $\psi = -(1/3)\ln 2 = 0.231$. In the present model, $\psi = (1/6)\ln\theta - (1/3)\ln\left(1+\xi^{\pm 3}\right)$.

To calculate ψ we used the extensive dataset of diameters, lengths and distensibilities of arteries provided in Ref. [24]. We kept the identification number of the each arterial segments used in Fig. 2 and Table 2 of Ref. [24]. The ratio of lengths $\xi = L_2 / L_1$ respects to arterial segments that converge at a bifurcation. On the values given in Ref. [24] we have no absolute guarantee that some of these segments do not have small (or very small) intermediate branches.

This can occur especially in very long segments in which it is likely to find small branches not represented in Fig. 2 and Table 2 of Ref. [24]. A sign of this is that the proximal and distal diameters of these segments differ a lot. For this reason, the data for lengths of arterial segments are used with some caution. We chose arterial segments that correspond to dichotomous branching in which parent and daughter vessels are clearly defined. In total 22 arteries were included in the calculation of ψ.

Table 2.1 Diameter scaling between parent and daughter human arterial segments, as observed, and predicted through ψ by the scaling relations defined by Murray's law, WBE model, and present model (see Eq. (2.34)).

Artery	Distensibility coefficient (Pa^{-1})	Diameter (mm)	Lenght (mm)	x	ξ	ψ_{observ}	ψ_{Murray}	ψ_{WBE}	ψ this model
4 subclavian A	2.176	9.0	34.0	3.778	0.353				
7 subclavian B	1.643	8.1	422.0	52.099		-0.105	-0.231	-0.347	-0.016
6 vertebral	1.095	3.7	149.0	40.270		-0.889	-0.231	-0.347	-1.057
7 subclavian B	1.643	4.7	422.0	89.787	0.285				
8 radial	1.118	3.7	235.0	63.514		-0.239	-0.231	-0.347	-0.008
9 ulnar A	1.148	3.7	67.0	18.108		-0.239	-0.231	-0.347	-1.262
9 ulnar A	1.148	3.4	67.0	19.706	2.165				
10 interosseous	0.810	2.1	79.0	37.619		-0.482	-0.231	-0.347	-0.804
11 ulnar B	1.043	3.2	171.0	53.438		-0.061	-0.231	-0.347	-0.032
14 aortic arch 2	3.361	20.8	39.0	1.875	0.654				
18 thoracic aorta 1	3.196	18.9	52.0	2.751		-0.096	-0.231	-0.347	-0-082
19 subclavian A	2.108	11.0	34.0	3.091		-0.637	-0.231	-0.347	-0.507
41 abdominal aorta	2.221	10.4	20.0	1.923	1.000				
42 common iliac	1.793	7.9	59.0	7.468		-0.275	-0.231	-0.347	-0.231
43 common iliac	1.793	7.9	59.0	7.468		-0.275	-0.231	-0.347	-0.231
42 common iliac	1.793	7.0	59.0	8.429	0.347				
50 external iliac	1.613	6.4	144.0	22.500		-0-090	-0.231	-0.347	-0.014
51 inner iliac	1.238	4.0	50.0	12.500		-0.560	-0.231	-0.347	-1.070
37 abdominal aorta C	2.371	11.8	20.0	1.695	3.313				
38 renal	1.448	5.2	32.0	6.154		-0.819	-0.231	-0.347	-1.207
39 abdominal aorta D	2.303	11.6	106.0	9.138		-0.017	-0.231	-0.347	-0.009
50 external iliac	1.613	6.1	144.0	23.607	0.284				
52 femoral	1.328	5.2	443.0	85.192		-0.160	-0.231	-0.347	-0.008
53 deep femoral	1.208	4.0	126.0	31.500		-0.422	-0.231	-0.347	-1.266
52 femoral	1.328	3.8	443.0	116.579	0.936				
55 anterior tibial	0.930	2.6	343.0	131.923		-0.379	-0.231	-0.347	-0.199
54 posterior tibial	1.035	3.1	321.0	103.548		-0.204	-0.231	-0.347	-0.265

Table 2.1 presents the ψ values as predicted by Murray's law, the WBE model, and the present model. For the most part of the cases the present model predicts the observed values with better approximation than Murrays' law, or the WBE model. This is especially true for the cases of asymmetric branching. The cases in which predictions deviate a lot from the observed values respect to very long vessels, i.e. those that are likely to present very small branches not considered in the dataset used.

Based on the present model, a recently published study of the arterial structure [25] also showed that, in general arterial lengths are not optimized with respect to hemodynamic performance, and then an explanation was offered for the elongation of the ascending aorta in healthy people during lifetime. The same study also showed that impedance of the ascending aorta, descending aorta and carotid artery decreases during body growth, therefore suggesting a trend for improvement of hemodynamic performance during that period of life.

2.4 Conclusions

In this study, based on the minimization of global impedance, the scaling laws of lengths and diameters of the parent and daughter channels in a branching channel are generalized to the case of pulsatile flow.

It is shown that in case of constant tree volume, scaling depends both upon the pulse frequency and the branching asymmetry. Another important parameter that influences optimal scaling is the coefficient of distensibility of the channel walls, which is a parameter widely used in the characterization of the arteries in the circulatory tree.

In the limit of zero pulse frequency these scaling laws match Murray’s law of diameters and also the scaling laws of lengths of branching channels with minimal global flow resistance under the existing constraints.

We also show that if the additional constraint of constant global pressure head is imposed to the flow in parent and daughter channels, the optimal ratio of daughter to parent channels lengths follows a law similar to that of channel diameters.

In case that the daughter channel has lower relative distensibility global impedance decreases with pulse frequency. Conversely, if the daughter channel is more distensible pulse frequency increases impedance as the pulse frequency falls in the vicinity of the characteristic frequency of the parent channel.

The effect of the relative distensibility of parent and daughter channels is shown to be important. In this way, the channel with lower relative distensibility must have their diameter increased to perform optimally, i.e. to achieve minimal impedance.

For the case of the human arterial trees, the predictions of the present model were compared with those of Murray's law, and the WBE model, and especially in the cases of asymmetric branching provided a better approximation to the observed values.

Acknowledgement

The authors acknowledge the funding provided by the CGE, under the contract Pest/OE/CTE/UI0078/2014, with FCT (the Portuguese Science and Technology Foundation).

Appendix

The impedance is represented by a phase vector (phasor), **Z**. For a channel that branches in two different channels (Fig.2.1) the overall impedance reads.

$$Z_T = Z_0 + \left(Z_1^{-1} + Z_2^{-1} \right)^{-1}, \tag{A1}$$

where $Z_i = R_i / \left(1 + j\omega R_i C_i\right)$, i=0, 1, 2, and with $j = \sqrt{-1}$. In polar coordinates, the generic phasor reads:

$$Z_i = \left|Z_i\right| \left(\cos\phi_i + j \sin\phi_i\right), \tag{A2}$$

with $\phi_i = \arctan(\omega R_i C_i)$. For the flow system of Fig. 2.1, from Eqs.(2.7) and (2.8), we get

$$\phi_i = \arctan(32\omega x \beta \mu), \tag{A3}$$

We assume that in (A2) the imaginary part of Z_i may be neglected if $\sin\phi_i$ is of order 10^{-2}. In that case, $\cos\phi_i \approx 1$. Then, for a flow system that condition implies

$$\omega x \beta \mu < 3.2 \times 10^{-4}. \tag{A4}$$

The inequality (A4) is verified for the vast majority of flow systems. For example, for the human arterial system, $\omega x \beta \mu \approx 10.10^{2}.10^{-5}.10^{-3} \approx 10^{-5}$.

Therefore, in such conditions, Eq.(A1) reduces to

$$|Z|_T \cong |Z|_0 + \left(|Z|_1^{-1} + |Z|_2^{-1} \right)^{-1}. \qquad \text{(A5)}$$

With $\sin\phi_i$ of order 10^{-2}, when the two members of (A5) are set equal, the associated relative error is of order 10^{-4}.

References

[1] C. D. Murray, "The Physiological Principle of Minimum Work. I. The vascular system and the cost of blood volume", *Proc. Nat. Ac. Sci. U. S. A.*, 12 (3): 207–214 (1926).

[2] C. D. Murray, "The Physiological Principle of Minimum Work. II. Oxygen exchange in capillaries", *Proc. Nat. Ac. Sci. U. S. A.,* 12 (5): 299–304 (1926).

[3] T. F. Sherman, "On connecting large vessels to small: The meaning of Murray's Law", *The Journal of General Physiology,* 78 (4): 431–453 (1981).

[4] A. Bejan, L. A. O. Rocha, S. Lorente, "T- and Y-shaped constructs of fluid streams", *International Journal of Thermal Sciences*, 39: 949–960 (2000).

[5] G.B. West, J.H Brown, & B.J. Enquist, "A general model for the origin of allometric scaling laws in biology", *Science,* 276: 122–126 (1997).

[6] A. Bejan, *Shape and Structure, from Engineering to Nature*, Cambridge University Press, Cambridge, 1-314 (2000).

[7] A. Bejan, *Advanced Engineering Thermodynamics*, 3rd ed., Wiley, Hoboken, (2006), 840-841.

[8] A. H. Reis, A. F. Miguel, M. Aydin, Constructal Theory of flow architectures of the lungs, *Medical Physics*, 31 (5): 1135-1140 (2004).

[9] A. H. Reis, Constructal Theory: From engineering to Physics, and how flow systems develop shape and structure, *Applied Mechanics Reviews*, 59: 269-282 (2006).

[10] A. Bejan and S. Lorente, *Design with Constructal Theory*, Wiley, Hoboken, N. York, (2008), 1-490.

[11] B. Mauroy, M. Filoche, E. R. Weibel, B. Sapoval, "An optimal bronchial tree may be dangerous", *Nature,* 427: 633-636 (2004).

[12] M. Florens, B. Sapoval and M. Filoche, “Optimal branching asymmetry of hydrodynamic pulsatile trees”, *Phys. Rev. Lett*., 106: 178104 (2011).

[13] C. Mavroudis, “To pulse or not to pulse”, *The Annals of Thoracic Surgery,* 25: 259-271 (1978).

[14] K. M. Taylor, W. H. Bain, K. G. Davidson, M. A. Turner, “Comparative clinical study of pulsatile and non-pulsatile perfusion in 350 consecutive patients”, *Thorax,* 37: 324-330 (1982).

[15] J. R. Womersley, "Method for the calculation of velocity, rate of flow and viscous drag in arteries when the pressure gradient is known, *Journal of Physiology,* 127: 553-563 (1955).

[16] D. N. Ku, “Blood flow in arteries”, *Annual Reviews of Fluid Mechanics*, 29: 399-434 (1997).

[17] D. A. Nield, A. V. Kuznetsov, “Forced convection with laminar pulsating flow in a channel or tube”, *International Journal of Thermal Sciences*, 46 (6): 551–560 (2007).

[18] R. Siegel, M. Perlmutter, “Heat transfer for pulsating laminar duct flow”, *ASME Journal of Heat Transfer*, 84 (2): 111–122 (1962).

[19] M. Faghri, K. Javadani, A. Faghri, “Heat transfer with laminar pulsating flow in a pipe”, *Letters in Heat and Mass Transfer*, 6 (4): 259–270 (1979).

[20] J. E Tsitlik, H. R. Halperin, A. S. Popel, A. A. Shoukas, F. C. P. Yin, N. Westerhof, “Modeling the circulation with three-terminal electrical networks containing special non-linear capacitors”, *Annals of Biomedical Engineering*, 20: 595-616 (1992).

[21] A. P. Avolio, “Multi-branched model of the human arterial system”, *Medical & Biological Engineering & Computing*, 18: 709-718 (1980).

[22] M. R. Mirzaee, O. Ghasemalizadeh, B. Firoozabadi, “Exact Simulating of Human Arteries using Lumped Model and Probing Constriction in Femoral and Carotid Arteries”, *American Journal of Applied Sciences*, 6 (5): 834-842 (2009).

[23] G.N. Jager, N. Westerhof, A. Noordergraaf, “Oscillatory flow impedance in electrical analog of arterial system: representation of sleeve effect and non-Newtonian properties of blood”, *Circ. Res*. 16: 121-133 (1965).

[24] P. Reymond, F. Merenda, F. Perren, D. Rüfenacht, N. Stergiopulos, “Validation of a one-dimensional model of the systemic arterial tree”, *Am. J. Physiol. Heart Circ. Physiol.* 297: H208-H222 (2009).

[25] C. Silva, A.H. Reis, “Structure and adaptation of arteries to pulsatile flow e the case of the ascending aorta”, Med. Phys. 41 (6) 063701 (2014)

CHAPTER 3

Structure and adaption of arteries to pulsatile flow – The case of the ascending aorta*

Purpose

The objectives are: i) assess the development of the impedance of some arteries during the first decades of life; ii) determine the influence of pulse rate in arterial impedance; iii) compare the structure of some arterial segments with optimized structures with respect to blood flow; iv) explain the elongation of the lifelong ascending aorta in healthy subjects.

Methods

A model of the arterial network previously developed by the authors, together with data of lengths, diameters, and distensibilities of arterial segments reported in the literature were used. The impedances of the aorta and carotid artery were calculated based on that model. Similarly, the impedances of various arteries corresponding to heart rates of 65 b.p.m. and 120 b.p.m. were calculated. Values observed in arterial segments were compared with the respective optimal values from the viewpoint of hemodynamic performance. This allowed drawing conclusions on the arterial segments that might be critical with regard to hemodynamics.

*Carla Silva and A. Heitor Reis, "Structure and adaptation of arteries to pulsatile flow: The case of the ascending aorta", *Med. Phys.* 41, 063701 (2014).

Results

It was found that in healthy people impedances of the aorta and the carotid artery decrease markedly with age especially during body growth. It was also found that impedances of the main arteries do not significantly change with heart rate, even if sharp changes in arterial distensibility are observed. With respect to optimal flow performance, it was found that scaling between diameters of branching arteries is generally close to optimality, while the corresponding length scaling is far from optimality. It was also found that the ascending aorta and aortic arch are among those arterial segments whose lengths are much smaller than the optimum values. An explanation is offered for the age associated elongation of the aorta in healthy people.

Conclusions

In healthy subjects the human arterial system continues to optimize its performance at least until the age of 60. [http://dx.doi.org/10.1016/j.jbiomech.2014.07.025]

Keywords: adaptation arteries pulsatile flow, elongation ascending aorta.

3.1 Introduction

As part of the circulatory system, the heart rhythmically pumps blood throughout the arterial tree. In the arterial tree of chordate animals the flow of blood is pulsatile in the sense that flow rate varies periodically around a mean value.

We may question whether pulsatile flow presents advantages over continuous flow in the transport of blood to tissues? Indeed we can point to at least two reasons: (1) Studies have shown the benefits of pulsatile flow in kidney function, lymph flow, and oxygen consumption, which are increased during pulsatile perfusion [1,2]; (2) pulsatile flow with distention of the arterial wall allows reducing peak pressure and also the energy expended by the heart to pump blood. Because the arterial wall distends during the propagation of the peak of the pressure wave, thereby increasing the cross section of the vessel, not only the flow resistance is reduced as also it allows storage of elastic energy, which makes it possible to maintain a negative gradient along the vessel needed to keep the flow subsequent to systole. This is especially true for the arteries that accommodate blood surging from the left ventricles during systole (aorta,

brachiocephalic, right and left common carotid arteries, right and left subclavian arteries, right and left vertebral arteries, right and left common iliac arteries) (see ref. [3]).

Besides, blood also presents unique rheological properties. In fact, blood viscosity decreases with shear rate. This attribute together with dilation of the arterial wall which is increased at the sites of high shear rate (through production of nitric oxide) facilitates blood flow when it is at peak. These features are part of a much complex control system that operates on the cardiovascular system through the conjugate action of the cardio-acceleratory, cardio-inhibitory, and vasomotor centers, and that provides blood to individual organs and tissues according to immediate needs.

The human circulatory system operates under a large set of constraints, ranging from the shape of the body, the location of its organs and tissues to the temporary needs related to physiology or human activity. Many works have been devoted to modeling of the circulatory system (see for instance refs. [4-10], and namely in recent years [3,11-13].

Here we analyze what would be the optimal structure of certain parts of the human circulatory system as if it had the freedom to change their morphology to optimize its performance. To carry out this exercise is important because freedom to morph exists at some degree during growth in childhood and adolescence, and also during the entire lifetime in some vessels that are not specially constrained by the nearby organs and tissues as it is the case of the ascending aorta. As we show in this paper, it seems likely the shape of the ascending aorta is adjusted during lifetime in order to facilitate blood flow.

We also analyze the importance of pulsatile flow frequency on blood flow impedance. With this purpose we use the resistive-capacitive (RC) model developed by Silva and Reis [14] which provides relationships that involve pulse frequency (heart rate), vessel diameter and length, arterial distensibility, and blood viscosity.

3.2 Blood flow impedance throughout lifetime

In the case of pulsatile flow in a vessel, the ratio of inlet/outlet pressure difference to flow rate measures its impedance, i.e. the extent to which the vessel resists the passage of a pulsed flow of blood. In case of a vessel of diameter *D* and length *L*, (aspect ratio $x = L / D$) with pulsatile flow of radial frequency ω, impedance reads (see ref. [14]):

$$|Z| = k_A x y^{-1} \left(1 + \omega^2 / \hat{\omega}^2\right)^{-1/2}, \tag{3.1}$$

where $k_A = 128\mu / \pi$, μ is dynamic viscosity of the fluid, $y = D^3$, $k = k_A \pi \beta / 4$, $\beta = (2/D)(\partial D / \partial P)$ is the distensibility coefficient of the vessel wall, *P* is pressure, and $\hat{\omega} = 1 / kx^2$ represents the characteristic frequency of the vessel. From Eq. (3.1) it is evident that impedance decreases with frequency (heart rate) and vessel diameter, and increases with vessel length and characteristic frequency. Because characteristic frequency varies inversely with β, impedance decreases with the distensibility coefficient of the vessel wall, therefore showing the importance of this parameter to ease blood flow.

Impedance as calculated from Eq. (3.1) results from a RC model of pulsatile flow [14] based on the Navier-Stokes equation for unidirectional flow: $\partial u / \partial t + u.grad\ u = -\rho^{-1} grad\ P + \nu\, lap\ u$, in which the inertial terms have been discarded because they are, at least, of one order of magnitude smaller than the other terms, as it is shown through scale analysis. In this way, let *u* denote average blood velocity, τ characteristic time related to pulse wave frequency, L_c the characteristic length in the flow direction, *D* vessel diameter, ρ blood density, ΔP pressure variation along the vessel and ν blood kinematic viscosity. Then, by assuming the following scale values for large arteries: $u \sim 10^{-1} ms^{-1}$, $\tau \sim 1s$, $L_c \sim 1m$, $D \sim 10^{-3} m$, $\Delta P \sim 10^3 Pa$ and $\nu \sim 10^{-5} m^2 s^{-1}$, the orders of magnitude (in ms^{-2}) of the terms in the Navier-Stokes equation are: $\partial u / \partial t \sim 10^{-1}$, $u.gradu \sim 10^{-2}$, $\rho^{-1} gradP \sim 1$, $\nu lap\ u \sim 1$, therefore justifying the use of the RC model [14] as a first approach in the study of the human arterial system. Models that include the term $\partial u / \partial t$ lead to greater complexity in the

calculations but did not cause a change in the conclusions. For example, the RLC model developed by Jager and co-workers [5] accounts for the "sleeve effect", which arises from the interaction between viscous and inertial terms in the Navier-Stokes equation. However, in the same study [5] it was shown that the "sleeve effect" is important in some arteries at frequencies higher than 15 rad s^{-1}, which is somehow beyond the normal range of the human pulse frequency.

Therefore, Eq. (3.1) enables calculation of blood flow impedances of some arteries for which data are available, namely the aorta and the carotid artery. With this purpose we used the normal values of cross-sectional area and distensibility of the aortas of healthy children and young adults that serve as a reference for the detection of pathological changes of the aorta in case of disease [15]. We also used data of normal length of the aorta of healthy adults (aged from 19 to 79 years), which exhibits a nearly linear increase with age [16] therefore allowing the estimation of the values in the range 0-18 years.

With respect to the carotid artery we used data of normal diameters [17] and distensibilities [18], and of normal lengths [16] found in the literature. Blood viscosity changes with shear stress, therefore is not easy to assign it a definite value in pulsatile flow. However, we used the values in ref. [19] to assign an average value to each vessel, according to the respective diameter. The heart rate considered was 65 beats per minute (b.p.m.). The relative error affecting the calculation of impedances is given by: $\left|(\Delta Z)/|Z|\right| \approx \left|(4\Delta D)/D\right| + \left|(\Delta L)/L\right| + \left|\left[(\Delta\hat{\omega})/\hat{\omega}\right](\omega/\hat{\omega})^2\right|$. Because $(\omega/\hat{\omega})^2 \sim 10^{-4}$, the contribution of the characteristic frequency to the error may be neglected. The relative error $(\Delta D)/D$ is of order 10^{-1} (see [15], [17]), while $(\Delta L)/L$ is of order 10^{-1} or smaller [16].

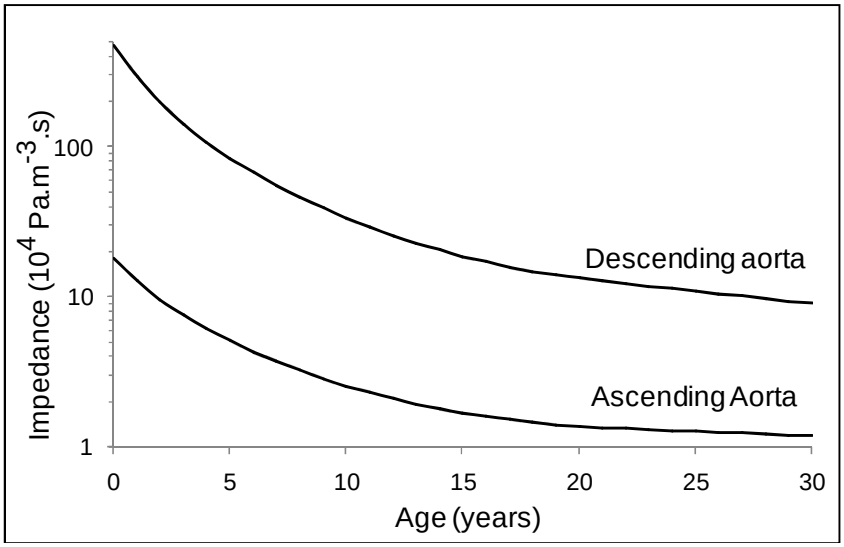

Fig. 3.1 Impedances of the ascending aorta and the descending aorta between birth and thirty years of age.

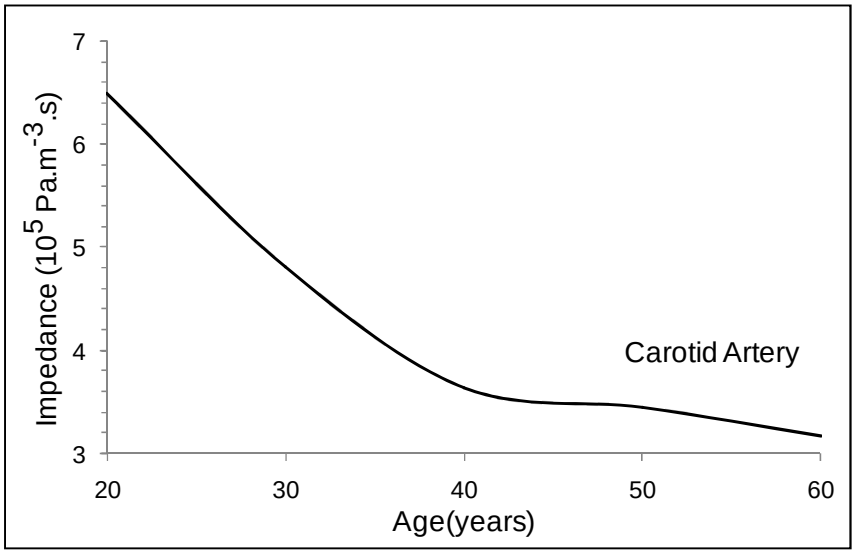

Fig. 3 2 Impedances of the carotid artery between twenty and sixty years of age.

Therefore, the relative error affecting the impedances calculated from Eq. (3.1) may reach 50%. However, this exercise is important because it allows verify if changes in impedance of the aorta of healthy humans occur during lifetime. The results for the ascending aorta, the descending aorta, and the carotid artery are shown in Figs. 3.1 and 3.2, respectively.

It is shown that the descending aorta presents the highest relative impedance, followed by the carotid, and then by the ascending aorta. In fact, this hierarchy of impedances was expected because, in a flow tree, daughter vessels present impedances higher than that of parent vessel.

We also observe that in healthy humans the impedances of theses arteries noticeably decrease with age, a trend that due to the magnitude of the values involved is not invalidated by the somewhat high relative error affecting the calculations. However, there are some differences: the impedances of both the ascending and the descending aorta show a continuous reduction that is very pronounced during growth of the human body (0-20 years), and less marked between 20 and 30 years of age. Due to lack of data we were not able to estimate aorta impedances subsequent to the third decade of life. After birth and until the fourth decade, the impedance of the carotid decreases linearly with age, and then it keeps decreasing until the age of 60.

O'Rourke, J. Hashimoto [11] found that at all heart rates the average ascending aortic impedance at the age of 80 is higher than at the age of 20. In fact, our study on impedance of the ascending aorta is focused on the period between birth and the age of 30. What our results show (Fig. 3.1) is that in healthy people the ascending aortic impedance decreases in that period. We believe that at the age of 80 arterial stiffening (together other aging processes) dominates over the processes that might be in place to improve arterial performance.

Then a question arises: why the impedances of the main vessels decrease with age? One can find a rationalization in the thought that Nature optimizes the human arterial tree in time, as it is observed in many natural systems. In fact, there is a large body of works that point to this direction. This tendency was summarized in a principle of maximization of “global flow access” known as the Constructal Law, which was first put forward in 1997 by Bejan [20] in the form: “For a finite-size system to persist in time (to live), it must evolve in such a way that it provides easier access to the imposed (global) currents that flow through it”. The Constructal Law entails generation of flow configuration such that it provides the highest global conductivity compatible with the existing constraints, and has successfully explained shapes and patterns of many both animate [21,22] and inanimate [23-25] systems (see also some Constructal Law reviews [26-29]).

3.3 Pulse frequency and blood flow impedance in the peripheral arteries

Another aspect that deserves attention is the importance of pulse frequency on impedance. By using Eq. (3.1) together with the data of diameter, length and distensibility of each vessel provided in ref. [3] to study the influence of pulse frequency on the arterial impedance of 43 arterial segments. The study was conducted through comparing arterial impedances corresponding to 65 and 120 b.p.m..

By using vessel distensibilities presented in ref. [3], for the most part of the arteries studied no noticeable differences were found in the respective impedances at each of these heart rates. This is due to the fact that the characteristic frequency $\hat{\omega}$ is much higher than 65 b.p.m., i.e. $\omega/\hat{\omega}$<<1. The few exceptions found, respect to some peripheral arteries (subclavian, radial, femoral, ulnar, posterior tibial, anterior tibial) whose impedances decreased significantly as heart rate changed from 65 to 120 b.p.m. (see Table 3.1).

As in the case of Figs. 3.1 and 3.2, the relative error affecting the impedances in Table 3.1 is of order 50%, mainly due to the contributions of the relative errors respecting to arterial diameters and lengths. However, the trend observed when the heart rate changes from 65 b.p.m. to 120 b.p.m. is due mainly to the term $\left|[(\Delta\hat{\omega})/\hat{\omega}](\omega/\hat{\omega})^2\right|$, for the reason that the characteristic frequency of the arteries in Table 3.1 is now close to the radial frequency ω corresponding to 120 b.p.m..

Table 3.1 Arterial impedances (Pa m^{-3} s) of some peripheral arteries as function of heart rate.

	Heart Rate	
Arteries	**65 b.p.m.**	**120 b.p.m.**
subclavian B	2.3937E+07	2.3840E+07
radial	4.5824E+08	4.5403E+08
femoral	1.9486E+08	1.8873E+08
ulnar B	7.2940E+08	7.2500E+08
posterior tibial	1.5063E+09	1.3992E+09
anterior tibial	3.3816E+09	2.8940E+09

Especially, the decrease in impedance is higher in the major arteries of the legs (femoral, posterior tibial, anterior tibial). However, some studies show that arterial distensibility decrease with heart rate [30,31]. Unfortunately, few data relating distensibility with heart rate are found in the literature. With regard to peripheral arteries data of the distensibilities of the radial and carotid arteries corresponding to 63, 90, and 110 b.p.m. were found in a seminal study by Giannattasio and co-workers [30]. If those data are used in Eq. (3.1) it is found that both the radial and carotid artery impedances do not change significantly from 63 to 110 b.p.m.. An explanation based on performance optimization that involves the characteristics of the end capillaries of the tissues bathed by those arteries will be provided in a next paper by the authors.

3.4 Optimal design versus actual shape of the arteries

Murray's Law [32-34] which states that the "cube of the radius of a parent vessel equals the sum of the cubes of the radii of the daughters" stays as a landmark scaling law of geometries of branching channels with non-turbulent flows was originally proposed by Cecil D. Murray (1926) for the circulatory and respiratory systems, but was later proven to be valid for all laminar branching flows [3,4,21,27].

In a previous work [14], based on minimization of global impedances, the authors derived scaling laws that generalize Murray's law for branching pulsatile flow. Hence, with respect to diameters the optimal scaling reads:

$$\frac{D_1}{D_0}=\theta^{1/6}\left(1+\xi^3\right)^{-1/3}, \qquad \frac{D_2}{D_0}=\theta^{1/6}\left(1+\xi^{-3}\right)^{-1/3}, \tag{3.2}$$

where D_0 is diameter of parent vessel, while D_1 and D_2 refer to diameters of daughter vessels, and

$$\theta=\left(2A_i^{-3/2}-A_i^{-1/2}\right)\Big/\left(2A_0^{-3/2}-A_0^{-1/2}\right), i=1,2\ , \tag{3.3}$$

with $A_i=1+\omega^2k_i^2x_i^4$, $i=0,1,2$, and $\xi=L_2/L_1$ standing for branching asymmetry.

In a similar way, optimal scaling for artery lengths reads:

$$\frac{L_1}{L_o}=\phi\left(1+\xi^3\right)^{-1/3}, \qquad \frac{L_2}{L_o}=\phi\left(1+\xi^{-3}\right)^{-1/3}, \tag{3.4}$$

where L_0 is length of parent vessel, L_1 and L_2 refer to lengths of daughter vessels, and

$$\phi=\theta^{2/3}\left(\frac{A_1}{A_0}\right)^{1/2}. \tag{3.5}$$

As discussed in §3.3, except for some peripheral arteries (subclavian, radial, femoral, ulnar, posterior tibial, anterior tibial) the characteristic frequency $\hat{\omega}$ is much higher than that corresponding to 65 b.p.m., i.e. $\omega/\hat{\omega}$<<1, and therefore optimal scaling is not much different from that of continuous flow. However, in Eq. (3.2) and Eq. (3.4), the asymmetry parameter ξ assigns smaller diameters and lengths, respectively, to the smaller daughter arteries. In effect, from Eq. (3.2) and Eq. (3.4), one obtains:

$$\frac{D_2}{D_1}=\frac{L_2}{L_1}=\xi. \tag{3.6}$$

We tested the scaling laws [Eqs (3.2) and (3.4)] by using the real values of various arterial bifurcations. For this purpose we used the extensive dataset of diameters, lengths and distensibilities of arteries provided in ref. [3]. We kept the identification number of the various arterial segments used in Fig. 3.2 and Table 3.2 of ref. [3]. The lengths in Eq. (3.4) respect to arterial segments that converge at a bifurcation. On the values given in ref. [3] we have no absolute guarantee that some of these segments do not have small (or very small) intermediate branches. This can occur especially in very long segments in which it is likely to find small branches. A sign of this is that the proximal and distal diameters of these segments differ a lot. For this reason, the data for lengths of arterial segments are used with some caution. Because the relative error affecting data of both diameters and lengths is of order 10%, while ξ presents a relative error of same order, diameters and lengths of daughter vessels calculated through Eq. (3.2) and Eq. (3.4) is of order 20%. The results are shown in Table 3.2.

In general, the diameters of daughter vessels calculated through Eqs. (3.2) are close to the measured ones. Yet, there are some exceptions (ulnar A, inner iliac, deep femoral, external carotid, and “sup. thy. asc. ph. lyng. fac. occ”). These daughter vessels have long parent vessels which may have small branchings, and therefore the respective data lengths might not be eligible in terms of the Eqs. (3.2).

We also evaluated optimal length scaling and compared the calculated lengths of daughter vessels with the real ones. Here we can observe few agreements together with many discrepancies. As discussed before, there is some uncertainty about the data of lengths of the arterial segments used in the calculation, namely if they correspond to segment free of small lateral branchings. This is especially true for the longer segments, as for instance the femoral artery (443 mm) in which the proximal diameter (5.2 mm) is much different from the distal diameter (3.8 mm) therefore indicating that many small branchings are likely to occur along the artery.

Table 3.2 Observed average diameters and lengths of parent (in bold) and daughter vessels (within brackets), and values of daughter vessels (in italic) for optimal hemodynamic performance. The numbers identify vessels according to the scheme in ref. [3]. (p) -proximal diameter, (d) - distal diameter.

Artery	Diameter (mm)	Lenght (mm)	Artery	Diameter (mm)	Length (mm)
3 brachiocephalic (d)	**18.0**	**34**	50 external iliac (d)	**6.1**	**144**
4 subclavian A (p)	*6.4* [11.5]	*12.1* [34]	52 femoral (p)	*5.8* [5.2]	*138.3* [443]
5 common carotid (p)	*17.7* [13.5]	*33.5* [94]	53 deep femoral (p)	*1.7* [4.0]	*39.3* [126]
4 subclavian A (d)	**9.0**	**34**	52 femoral (d)	**3.8**	**443**
7 subclavian B (p)	*8.8* [8.1]	*33.4* [422]	55 anterior tibial (p)	*2.8* [2.6]	*339.8* [343]
6 vertebral (p)	*3.1* [3.7]	*11.8* [149]	54 posterior tibial (p)	*2.7* [3.1]	*318.0* [321]
7 subclavian B (d)	**4.7**	**422**	15 common carotid (d)	**6.0**	**139**
8 radial (p)	*5.0* [3.7]	*441.8* [235]	16 internal carotid (p)	*6.0* [5.3]	*138.4* [178]
9 ulnar A (p)	*1.4* [3.7]	*125.9* [67]	17 external carotid (p)	*1.4* [4.7]	*31.9* [41]
9 ulnar A(d)	**3.4**	**67**	17 external carotid (d)	**4.3**	**41**
10 interosseous (p)	*1.5* [2.1]	*30.0* [79]	85 external carotid (p)	*2.4* [4.0]	*23.2* [61]
11 ulnar B (p)	*3.3* [3.2]	*64.9* [171]	86 sup. thy. asc. ph.lyng.(p)	*4.0* [2.0]	*38.4* [101]
14 aortic arch 2 (d)	**20.8**	**39**	85 external carotid(d)	**3.5**	**61**
18 thoracic aorta 1 (p)	*19.2* [19.0]	*35.9* [52]	89 superficial temporal (p)	*2.2* [3.2]	*37.5* [61]
19 subclavian A (p)	*12.5* [8.5]	*23.5* [34]	90 maxillary (p)	*3.2* [2.2]	*55.9* [91]
41 abdominal aorta (d)	**10.4**	**20**	89 superficial temporal (d)	**3.0**	**61**
42 common iliac (p)	*8.2* [7.9]	*15.9* [59]	93 superftemp frontal (p)	*2.4* [2.2]	*48* [100]
43 common iliac (left)(p)	*8.2* [7.9]	*15.9* [59]	94 superftemp parietal (p)	*2.4* [2.2]	*48,5* [101]
42 common iliac (d)	**7.0**	**59**	73 middle cerebral M1 (d)	**2.8**	**8**
50 external iliac (p)	*6.9* [6.4]	*58.2* [144]	74 MCA M2 sup. (p)	*2.2* [2.0]	*6.4* [71]
51 inner iliac (p)	*2.4* [4.0]	*20.2* [50]	75 MCA M" inf. (p)	*2.2* [2.0]	*6.3* [70]

The scaling defined by the equations (3.2) and (3.4) is optimized with respect to fluid (blood) dynamics only. However, many other constraints are in place, namely the distribution of organs in the body, together with their needs of blood supply, which were not considered in the derivation of those equations. Nevertheless, the exercise of comparing the actual values with the respective optimal values as regards blood flow is important since it identifies the arteries where blood flow is not optimized and where hemodynamics might affect arterial performance. Among such arterial segments are the ascending aorta, and the aortic arch that will be the object of the next section. In Table 3.2, we can identify other arterial segments that share such condition: common carotid, subclavian A, radial, ulnar A, inner iliac, deep femoral, external carotid, and “sup. thy. asc. ph. lyng. fac. occ. The segments that deviate from the optimal are likely to present increased hemodynamic resistances, namely through increased shear stresses affecting vessel walls. Interestingly, the human body has control mechanisms that deal with this problem through increased production of nitric oxide in the vessel walls where shear stress is higher [35].

3.5 The elongation of the ascending aorta

As referred before the ascending aorta is not optimized, as its length does not scale optimally [see Eq. (3.4)] with those of the aortic arch and the thoracic aorta A (see Fig. 3.3). In fact, while Eq. (3.4) calls for smaller lengths of daughter vessel segments with respect to parent ones, in the aorta occurs just the reverse. One may wonder why the chief vessel in the human body is not optimized with respect to blood flow. We believe that the special morphology of the aorta is the result of a trade-off among many objectives it has to comply with. In fact, in the small space allocated to it, the aorta has to divert the blood flow to the head, the arms, and organs in the thorax prior to redirecting the remaining flow to the rest of the body. This confers the aorta its special morphology, while it leaves it vulnerable to an extreme hemodynamic stress.

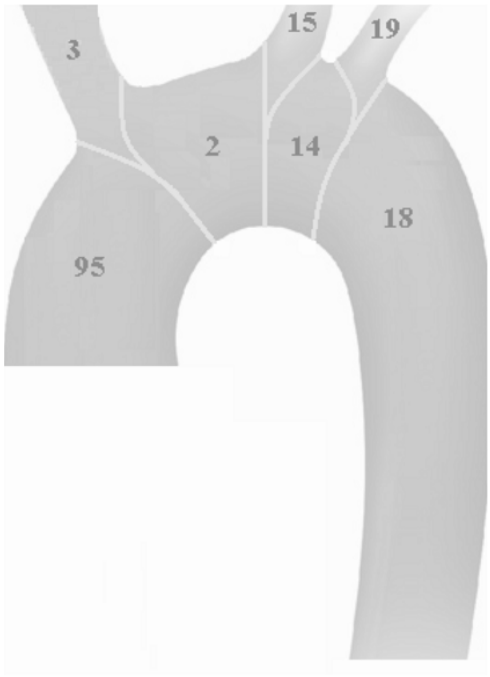

Fig. 3.3 Aorta segments and branches: 95 – ascending aorta; 3 – brachiocephalic; 2 – aortic arch A; 15 – common carotid; 14 – aortic arch B; 19 – subclavian A; 18 – thoracic aorta A. The numbers identify vessels according to the scheme in ref. [3].

To investigate the optimal morphology of the aorta with respect to hemodynamics we used Eq. (3.2) and Eq. (3.4). Then, by considering the diameter and length of the thoracic aorta, together with the diameter of the aortic arch B, we calculated the optimal length of the aortic arch B (See Fig. 3.3).

Then, in a similar way, by using the respective vessel diameter we successively calculated the lengths of the aortic arch A, and the ascending aorta. The values of the distensibilities, diameters and lengths of those vessels were taken from ref. [3]. The results are shown in Table 3.3.

We observe that in order to perform optimally all these arterial segments would have to be longer. This is especially noticeable for the aortic arch A - which would have to be more than three times longer - and the ascending aorta that should have its length doubled.

Table 3.3 Optimal average diameters and lengths of several segments of the aorta taking thoracic aorta A as the reference.

Artery	D (mm)	L (mm)	Lop (mm)
18 thoracic aorta A	19.5	52	…
14 aortic arch B	21.1	39	56.2
2 aortic arch A	24.6	20	65.5
95 ascending aorta	29.4	40	78.3

Studies on the variation of the length of the ascending aorta have shown that the aorta lengthens with age, even in healthy humans, primarily due to the elongation of the ascending aorta. The lengths of the descending aorta and carotid and iliac arteries were not associated with age [16]. In that study it was shown that the average length of the ascending aorta (defined as from aortic annulus to apex of arch) increased from 44 to 98 mm between 20 and 80 years of age, according to the regression formula $L = 0.9Y + 26.1\,mm$ where Y stands for years of age.

In a comment to these results O'Rourke and coworkers [36] suggested that the elongation of the ascending aorta was due to pulsatile strain in the longitudinal direction of the proximal aorta that is greater than pulsatile strain in the circumferential direction, therefore one would expect greater lengthening with age in the longitudinal direction than increase in diameter.

Here we offer an alternative explanation based on the fact that both the ascending aorta and the aortic arch are not optimized with respect to blood flow dynamics. Because, contrarily to other arterial segments that cannot morph in time for the reason that either they are associated to skeletal muscle or to bones of fixed length (as for instance the arteries: radial, ulnar A, inner iliac, deep femoral), the ascending aorta is quite free to morph because it is slightly constrained by adjacent tissues. As an approximate measure of the length from aortic annulus to apex of arch we add the optimal values of the aortic arch A and the ascending aorta to get 143.8 mm (see Table 3.3), value that is the reference for optimal hemodynamics (minimum impedance). Therefore, in our view the elongation of the ascending aorta corresponds to optimization of the aortic morphology during lifetime towards an increasingly better

hemodynamic performance. In this way, the aorta uses the freedom to morph for reducing the shear stresses associated to blood flow, and consequently the stresses that are induced in the arterial wall.

Morphing in time is a characteristic of the human body that seeks for better performance through adaptation either to external or internal constraints.

3.6 Conclusions

Based on data of arterial diameter and length, and distensibility coefficient after birth and at up to the age of thirty years it its shown that in healthy humans flow impedances of the ascending aorta and descending aorta decrease markedly in this period, while by using similar data for the period 0-60 years of age it is shown that impedance of the carotid artery keeps decreasing in this period.

It is also shown that flow impedances of arteries do not significantly change with heart rate. Despite distensibilities of some peripheral arteries - subclavian, radial, femoral, ulnar, posterior tibial, anterior tibial – decrease as heart rate increases from 65 to 120 b.p.m. their respective impedances do not significantly change with heart rate.

By applying the scaling laws for minimum flow impedance it is shown that artery diameters are in general quite close to the optimal values, while artery lengths are not. Among the arteries whose lengths are far from the optimal values are the ascending aorta, aortic arch, common carotid, subclavian A, radial, ulnar A, inner iliac, deep femoral, external carotid, and “sup. thy. asc. ph. lyng. fac. occ.”. This aspect was explained by the fact that arteries have to deliver blood to organs that are distributed in the body according to overall body performance, and therefore most of the times do not comply with optimal performance with respect to blood flow. On the other hand, may be subject to additional stresses because they are not optimized hemodynamically.

Finally, it is shown that the normal lengths of the ascending aorta and the aortic arch are smaller than their optimal lengths. The optimal length of the ascending aorta plus the aortic arch is found to be 143.8 mm. We interpreted the results of the study by Sugawara and co-workers [16] that showed that in healthy individuals the average length of the ascending aorta (defined as from aortic annulus to apex of arch)

increased from 44 to 98 mm between 20 and 80 years of age, as the tendency of this flow system to optimize its performance in time taking advantage of its freedom to morph due to be slightly constrained by adjacent tissues. This tendency has also been observed in many natural both animate and inanimate systems, and is known as the Constructal Law.

The results of this study may be extended to other animals provided that the relevant data are available.

Acknowledgement

The authors acknowledge the funding provided by the CGE, under the contract Pest/OE/CTE/UI0078/2014, with FCT (the Portuguese Science and Technology Foundation).

References

[1] C. Mavroudis, “To pulse or not to pulse”, *The Annals Thor. Surg.* 25 259-271 (1978).

[2] K. M. Taylor, W. H. Bain, K. G. Davidson, M. A. Turner, “Comparative clinical study of pulsatile and non-pulsatile perfusion in 350 consecutive patients”, *Thorax* 37, 324-330 (1982).

[3] P. Reymond, F. Merenda, F. Perren, D. Rüfenacht and N. Stergiopulos, “Validation of a one-dimensional model of the systemic arterial tree”, *Am. J. Physiol. Heart Circ. Physiol.* 297: H208–H222 (2009).

[4] J. R. Womersley, "Method for the calculation of velocity, rate of flow and viscous drag in arteries when the pressure gradient is known, *J. Physiology*, 127 553-563 (1955).

[5] G. N. Jager, N. Westerhof, A. Noordergraaf, “Oscillatory flow impedance in electrical analog of arterial system: representation of sleeve effect and non-Newtonian properties of blood”, *Circ. Res.,* 16:121-33 (1965).

[6] W. R. Milnor, C. R. Conti, K. B. Lewis, M. F. O'Rourke, “Pulmonary arterial pulse wave velocity and impedance in man”, Circ. Res., 25(6):637-49 (1969).

[7] W. R. Milnor, “Arterial impedance as ventricular afterload”, *Circ. Res*., 36(5): 565-570 (1975).

[8] A. P. Avolio, “Multi-branched model of the human arterial system”, *Med. & Bio. Eng. & Comp.*, 18, 709-718 (1980).

[9] J. E. Tsitlik, H. R. Halperin, A. S. Popel, A. A. Shoukas, F. C. P. Yin, N. Westerhof, “Modeling the circulation with three-terminal electrical networks containing special non-linear capacitors”, *Ann. Biomed. Eng.* 20: 595-616 (1992).

[10] D. N. Ku,”Blood flow in arteries”, *Ann. Rev. Fluid Mech*., 29, 399-434 (1997).

[11] M. F. O'Rourke, J. Hashimoto, “Mechanical Factors in Arterial Aging: A Clinical Perspective”, *J. Am. Coll. Cardiol*. 50(1):1-13 (2007).

[12] M. R. Mirzaee, O. Ghasemalizadeh, B. Firoozabadi, “Exact Simulating of Human Arteries using Lumped Model and Probing Constriction in Femoral and Carotid Arteries”, *Am. J. Appl.Sci*.6 (5) 834-842 (2009).

[13] M. Florens, B. Sapoval, M. Filoche, “Optimal branching asymmetry of hydrodynamic pulsatile trees”, *Phys. Rev. Lett.*,106: 178104 (2011).

[14] Carla Silva and A. Heitor Reis, “Scaling relations of branching pulsatile flows, *International Journal of Thermal Sciences*, 88, 77-83 (2015).

[15] I. Voges, M. Jerosch-Herold, J. Hedderich, E. Pardun, C. Hart, D. D. Gabbert, H. H. Kramer, C. Rickers, “Normal values of aortic dimensions, distensibility, and pulse wave velocity in children and young adults: a cross-sectional study”, *J. Cardiovasc Magn Reson*., 14 (Suppl 1), (2012).

[16] J. Sugawara, K. Hayashi, T. Yokoi, H. Tanaka, “Age-associated elongation of the ascending aorta in adults”, *J. Am. Coll. Cardiol. Img*., 1, 739 –48 (2008).

[17] A. R Ahlgren, F. Hansen, B. Sonesson, T. Lanne, “Stiffness and diameter of the common carotid artery and abdominal aorta in women”, *Ultrasound Med. Biol*., 23: 983-8 (1997).

[18] A. Benetos, S. Laurent, A. P. Hoeks, P. H. Boutouyrie, M. E. Safar, “Arterial alterations with aging and high blood pressure. A noninvasive study of carotid and femoral arteries”, *J. Am. Heart Assoc.-Arterioscl. Thromb. Vasc. Bio.*,13: 90-97 (1993).

[19] B. Canaud, I. Jaussent, A. Rodriguez, H. Leray-Moragues, L. Chenine, A. Picard, M. Morena, J. P. Cristol, “Whole-blood viscosity increases significantly in small arteries and capillaries in hemodiafiltration. Does acute hemorheological change trigger cardiovascular risk events in hemodialysis patient?”, *Hemodialysis International*, 14: 433–440 (2010).

[20] A. Bejan, *Advanced Engineering Thermodynamics*, 2nd ed. Wiley, New York, 1997, Ch. 13.

[21] A. H. Reis, A. F. Miguel, M. Aydin, “Constructal theory of flow architectures of the lungs”, *Med. Phys.,* 31 (5), 1135-1140 (2004).

[22] A. Bejan, S. Lorente, “The constructal law and the evolution of design in nature”, *Phys. Life Rev*., 8: 209-240 (2011).

[23] A. H. Reis, A. Bejan, “Constructal theory of global circulation and climate”, *Int. J. Heat Mass Transf.*, 49 (11-12): 1857 – 1875 (2006).

[24] A. H. Reis, “Constructal view of scaling laws of river basins”, *Geomorphology* 78, 201-206 (2006).

[25] A. H. Reis, C. Gama, “Sand size versus beachface slope - an explanation based on the Constructal Law”, *Geomorphology*, 114: 276–283 (2010).

[26] A. Bejan, *Shape and Structure, From Engineering to Nature*, Cambridge Univ. Press, Cambridge, UK, (2000).

[27] A. H. Reis, “Constructal Theory: From Engineering to Physics, and How Flow Systems Develop Shape and Structure”, *Appl. Mech. Rev*., 59: (5) 269-282 (2006).

[28] A. Bejan, S. Lorente, *Design with Constructal Theory*, Wiley, Hoboken, 2008.

[29] A. Bejan and S. Lorente, "Constructal law of design and evolution: Physics, biology, technology, and society", *J. Appl. Phys*., 113: 151301 (2013).

[30] C. Giannattasio, A. Vincenti, M. Failla, A. Capra, A. Ciro , S. De Ceglia, G. Gentile, R. Brambilla, G. Mancia, “Effects of heart rate changes on arterial distensibility in humans”, *Hypertension*, 42: 253–256 (2003).

[31] A. Pitcher, P. Leeson, C.Forfar, C. Trevitt, J.M. Francis, S. Neubauer, S. E. Petersen, “Aortic distensibility decreases during exercise in normal volunteers”, *J. Cardiov. Magn. Reson*., 12: 136 (2010).

[32] C. D. Murray, “The Physiological Principle of Minimum Work: I. The Vascular System and the Cost of Blood Volume”, *Proc. Nat. Ac. Sci. U. S. A.,*12 (3): 207–214 (1926).

[33] C. D. Murray, “The Physiological Principle of Minimum Work: II Oxygen Exchange in Capillaries”, *Proc. Nat. Ac. Sci. U. S. A*., 12 (5): 299–304 (1926).

[34] T. F. Sherman, “On connecting large vessels to small: The meaning of Murray's Law”, *The J. of Gen. Physiology*, 78 (4): 431–453 (1981).

[35] O. K. Baskurt, H. J. Meiselman, “Blood Rheology and Hemodynamics”, *Seminars in thrombosis and hemostasis*, 29: 435-450 (2003).

[36] M. O’Rourke, A. Farnsworth, J. O’Rourke, “Aortic Dimensions and Stiffness in Normal Adults”, *JACC: Cardiovascular Imaging*, 1, n.6, 749-751 (2008).

CHAPTER 4

Heart rate, arterial distensibility, and optimal performance of the arterial tree*

Abstract

In this study we explore the ability of a previously developed model of pulsatile flow for explaining the observed reduction of arterial distensibility with heart rate. The parameters relevant for the analysis are arterial wall distensibility together with permeability and reflection coefficients of the end capillaries. A non-specific artery and the ensemble of tissues supplied by that artery were considered in the model. The blood current within that artery was equalized to the sum of all microcurrents in the tissues supplied by that artery. A formula emerged that relates changes in arterial distensibility with heart rate, and also with some particular aspects of microcirculation. Then, that formula was tested with data of distensibilities of the radial and carotid arteries observed at the heart rates of 63, 90, and 110 b.p.m. The formula correctly predicted the trend of decreased distensibility with heart rate for both arteries. Moreover, due to the fact that the carotid artery supplies the brain, and because the Blood–Brain barrier is highly restrictive to colloids in the blood, for the carotid artery the formula predicted a less marked decrease in distensibility than in the case of the radial artery feeding muscle tissue, which has a greater permeability to colloids, a trend that was confirmed by data. It was found that reduction of arterial distensibility with heart rate was greater in arteries that supply end capillaries with high permeability and low reflection coefficients.

* Carla Silva, A. Heitor Reis, ”Heart rate, arterial distensibility, and optimal performance of the arterial tree”, Journal of Biomechanics, 47, 2878–2882 (2014).

Keywords: pulsatile flow, heart rate, arterial distensibility.

4.1 Introduction

It has been long recognized that pulsatile blood flow performs best than continuous flow because it induces lower total peripheral resistance and mean arterial pressure [1], and also better blood perfusion [2]. The distensibility coefficient of the vessel wall is defined as $\beta = (2/D)(\partial D/\partial P)$ where P is pressure within the vessel, and D is vessel diameter. Henceforth the term distensibility is used to mean distensibility coefficient.

On the other hand, a recent model of pulsatile flow predicts that if distensibility is kept constant, arterial impedance must decrease with pulse frequency [3]. Actually, if pulse frequency (heart rate) and therefore blood current is increases in response to needs of organs in the body, then it makes sense that arterial impedance is lowered to ease the access of blood. On the other hand, if arterial impedance decreases with distensibility [3] one would expect that increased blood current would lead to decreased arterial impedance with heart rate.

However, many studies have shown that in humans arterial distensibility varies inversely with heart rate [4-9]. The same effect has been observed in rats [10]. Though, according to the model above referred [3] increased heart rate leads to lower arterial impedance, the observed increased arterial stiffness with heart rate actually increases impedance. Apparently, this behavior does not make sense because easing blood flow is sought to be the objective of the circulatory system.

An extended search in the pertinent literature also revealed some studies that concluded that arterial stiffness was not affected by heart rate [11, 12]. However, these two studies have some particularities: in [11] arterial stiffness changes with heart rate were indirectly estimated through the augmentation index calculated from the blood pressure waveform, while in [12] arterial stiffness was "determined before and 10 min after graded arm-cycling exercise".

On the other hand some other studies [13, 14, 15] found that whole body arterial compliance (WBAC) and then arterial distensibility was increased after cycling and treadmill exercise with relation to the values prior to exercise. This is a different result

that compares arterial distensibility before and after the period in which heart rate is increased.

The decrease of arterial distensibility with heart rate is somewhat counter-intuitive, and challenges the current paradigm of human physiology. From the physiological point of view, no explanation has yet been presented. In the following we offer an explanation based on the assumption of optimal hemodynamic performance of the arterial tree, and show that increase in arterial stiffness with heart rate may be understood as the adjustment of the arterial tree on the way for global optimization of its performance. For this purpose we first take a closer look to microcirculation in the capillaries forming the end of the arterial tree.

4.2 Microcirculation and Starling forces

Blood is transported downstream in the arterial tree until it reaches the end capillaries that bridge arteriole and venule ends, which deliver it to the interstitial fluid that bathes every cell (see Fig. 4.1). Capillaries have opening of various widths according to the tissue to which blood is supplied. Many capillaries may turn impermeable to the bigger colloids in the blood, namely the proteins, therefore regulating their delivery to the interstitial fluid. Special classes of proteins called albumins constitute about 50% of human plasma protein and are very important as carriers of hydrophobic substances (e. g. lipid soluble hormones, bile salts, free fatty acids) [16]. Water and other small molecules are generally free to pass through capillary openings.

In this way, filtration occurs along the capillary driven by the difference in hydrostatic pressure $\Delta P_{ci} = P_c - P_i$ between the capillary (P_c) and the interstitial space (P_i), therefore increasing the concentration of colloids that are not allowed to pass into the interstitial fluid. As the result a colloid osmotic pressure - oncotic pressure difference $\Delta\Pi_{ci} = \Pi_c - \Pi_i$ - develops between the interstitial fluid and the blood within the capillaries, which opposes the pressure gradient that drives the blood from the capillaries to the interstitial space (i.e. the space between cells that is bathed by the interstitial fluid). Within the capillary, hydrostatic pressure decreases from P_a (at the end of the arteriole) to P_v (at the beginning of the venule), $\Delta P_c = P_a - P_v$.

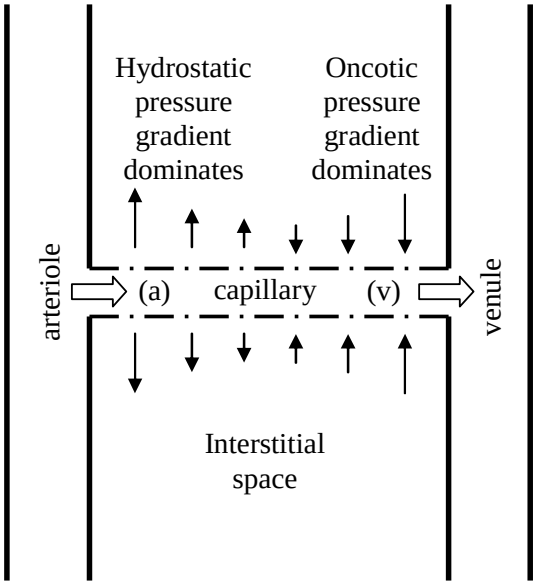

Fig. 4.1 Microcirculation: blood enters the capillary at the arteriolar end (a), water, salts and colloids are driven into the interstitial space by the capillary gradient, and return into the capillary driven by the oncotic gradient at the venular end (v).

Hence, the blood leaving the end of the arteriole splits into two currents: one of them flows within the interstitial space; another one flows within the capillary. Both currents merge together at the entrance of the venula.

The current flowing into the interstitial space may be described by Starling's equation [17, 18]:

$$i_{ci} = K_{ci}\Delta P_{ci} - \sigma_{ci}\Delta\Pi_{ci}\,, \tag{4.1}$$

where i_{ci} is the net current between the capillary and the interstitial space, k_{ci} and σ_{ci} respectively stand for filtration coefficient and reflection coefficient of the capillary section in which i_{ci} exists, Π_c and Π_i represent oncotic pressure of the colloids in the capillary and the interstitial space, respectively. Though in the literature, k_{ci} and σ_{ci} are termed "coefficients", in fact they represent conductances that are proportional to the extension of the capillary in which exchange of fluids occur. The reflection coefficient is null for a capillary wall permeable to all colloids in the blood. The first term in the r.h.s of equation (4.1) represents the current from the capillary to the interstitial space while the second one stands for the current from the interstitial space onto the capillary that is driven by oncotic pressure gradient. At the arteriolar end the hydrostatic driven current dominates, hence there is a net influx to the interstitial space, while the opposite occurs at the venular end where a net outflow towards the capillary (see Fig.4.2).

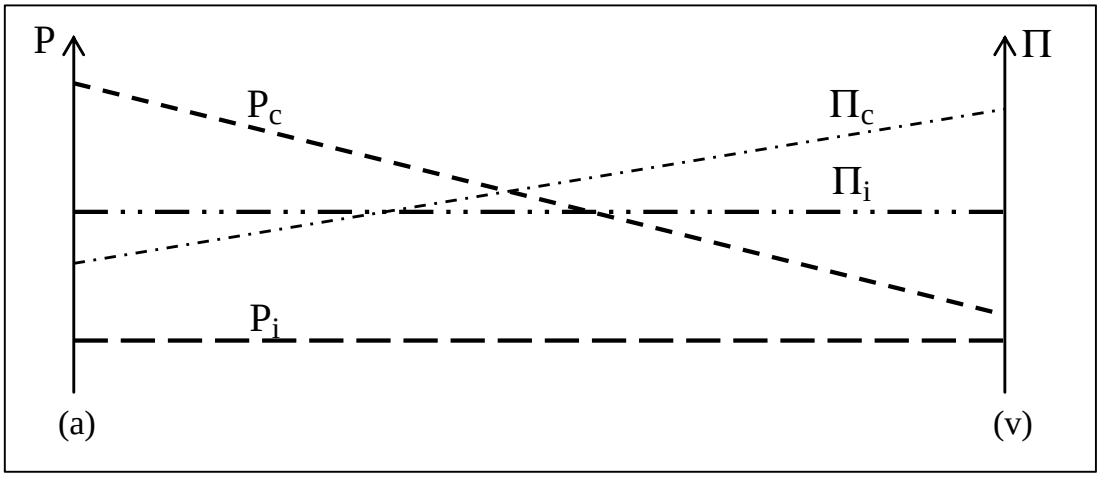

Fig. 4.2 Variation of capillary hydrostatic pressure (P_c), interstitial hydrostatic pressure (P_i), capillary oncotic pressure (Π_c), and interstitial oncotic pressure (Π_i), between arteriolar (a) and venular (v) ends of the capillary. Π_c increases within the capillary due to loss of fluid to the interstitial space. P_i and Π_i are constant in the interstitial space [17,18].

The current within the capillary is driven by the hydrostatic pressure difference $\Delta P_c = P_a - P_v$ and is given by:

$$i_c = \Delta P_c / Z_c , \tag{4.2}$$

where Z_c stands for capillary impedance. In this way, the total current leaving the arteriolar end is given by:

$$i = i_i + i_c = K_{ci}\Delta P_{ci} - \sigma_{ci}\Delta\Pi_{ci} + \Delta P_c / Z_c . \tag{4.3}$$

On the other hand, the total current entering the venular end is composed of the current from the interstitial space into the capillary:

$$i_v = i_{ic} + i_c = K_{ic}\left(\Delta P_c - \Delta P_{ci}\right) + \sigma_{ci}\Delta\Pi_{ci} + \Delta P_c / Z_c , \tag{4.4}$$

where $K_{ic} \neq K_{ci}$ and $\sigma_{ic} \neq \sigma_{ci}$ respectively stand for filtration coefficient and reflection coefficient of the capillary section in which i_{ci} exists. Note that here we have considered the general case in which $K_{ci} \neq K_{ic}$ and $\sigma_{ci} \neq \sigma_{ic}$. Additionally, due to mass conservation for the steady state one has:

$$i = i_v + i_{lymph} , \tag{4.5}$$

where i_{lymph} stands for the rate at which lymph is drained from the interstitial space to the lymphatic circulation. Therefore, from Eqs. (4.3-4.5) one obtains:

$$i_{lymph} = \left(K_{ic} + K_{ci}\right)\Delta P_{ci} - K_{ic}\Delta P_c - \left(\sigma_{ci} + \sigma_{ic}\right)\Delta\Pi_{ci}\,. \tag{4.6}$$

In the tissues that do not possess lymphatic circulation (e.g. brain, eyes) special overflow drainage systems allow for the removal of excess fluid [17].

4.3 Heart rate and optimal performance of the arterial tree

Let us consider an artery that feeds blood to the tissues downstream (Fig. 4.3). In an artery of diameter *D* and length *L*, (aspect ratio $x = L/D$), with pulsatile flow of frequency ω, under pressure difference ΔP the average current *I* reads (see [3]):

$$I = \Delta P / Z \text{, with } Z = k_A x y^{-1}\left(1 + \omega^2/\hat{\omega}^2\right)^{-1/2}, \tag{4.7}$$

where $k_A = 128\mu\pi^{-1}$, μ is dynamic viscosity of the fluid, $y = D^3$, $k = k_A\pi\beta/4$, $\beta = \left(2/D\right)\left(\partial D/\partial P\right)$ is the distensibility coefficient of the vessel wall, *P* is pressure, and $\hat{\omega} = 1/kx^2$ represents the characteristic frequency of the vessel.

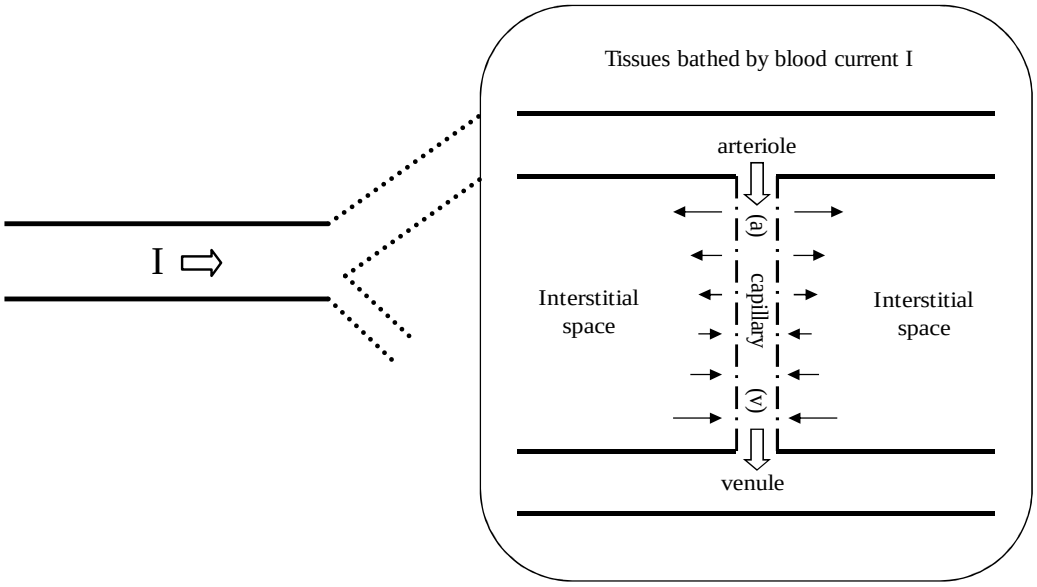

Fig. 4.3 Artery with blood current I and downstream tissues bathed by I. Exchange of blood components occurs through the capillary that connects arteriolar and venular ends.

The blood current I in that artery equals the sum of the blood currents leaving every arteriolar end in the tissues feed by that artery:

$$I = \sum_n i_n \,, \tag{4.8}$$

or, according to equation (4.3):

$$I = \sum_n \left(K_{ci} \Delta P_{ci} - \sigma_{ci} \Delta \Pi_{ci} + \Delta P_c / Z_c \right)_n \,. \tag{4.9}$$

The pressure drop along the capillary is proportional the absolute value of pressure drop along the artery, i.e. $\Delta P_c = \theta \Delta P$. For an optimally performing tree $\theta = 1$. In such a tree the same pressure drop occurs at level of branching (see [19]). In this way, by using Eqs. (4.5-4.9) one obtains:

$$Z^{-1} = \sum_n \left(\left[a_k \left(\sigma_{ci} + \sigma_{ic} \right) - \sigma_{ci} \right] \frac{\Delta \Pi_{ci}}{\Delta P} + a_k \frac{i_{lymph}}{\Delta P} + \theta \left(a_k K_{ic} + Z_c^{-1} \right) \right)_n \,, \tag{4.10}$$

where $a_k = K_{ci} \big/ \left(K_{ci} + K_{ic} \right)$. Besides we note that $Z_c \simeq R_c$ because the flow in capillaries is almost steady because in there the pressure wave is very much attenuated. As a consequence, the variation of the impedance with pulse rate is negligible, i.e. $\partial Z_c / \partial \omega \simeq 0$.

By taking the derivate of both member of Eq. (4.10) with respect to radial frequency ω one obtains:

$$\frac{f}{\beta} \frac{\partial \beta}{\partial f} \simeq -1 - \gamma \,, \tag{4.11}$$

with

$$\gamma = \sum_n \left(\left\{ \left[a_k \left(\sigma_{ci} + \sigma_{ic} \right) - \sigma_{ci} \right] \frac{\Delta \Pi}{\Delta P} + a_k \frac{i_{lymph}}{\Delta P} \right\} \frac{\hat{f}}{f} \left(1 + \frac{\hat{f}^2}{f^2} \right)^{1/2} \frac{Rf}{\Delta P} \frac{\partial (\Delta P)}{\partial f} \right)_n + \left(1 + \frac{\hat{f}^2}{f^2} \right) \beta \frac{f \partial P}{\partial f} \tag{4.11a}$$

where β is distensibility coefficient, $f = \omega / 2\pi$, $\hat{f} = \hat{\omega} / 2\pi$ stand for normal heart rate and characteristic frequency, respectively, and $R = k_A x y^{-1}$ stands for flow resistance of the artery [see Eq. (4.7)]. The last term in the r.h.s of Eq. (4.11a) depends on $\hat{f}^2 \big/ f^2$, which may be significant in some arteries (e.g. the carotid, see §4.4), and also on

$\partial P/\partial f$. However, the data in ref. [6] do not show a clear trend with respect to change in arterial pressure with heart rate, and more likely show that $\partial P/\partial f \sim 0$, therefore indicating that the last term in the r.h.s of Eq. (4.11a) may be neglected. In this way, γ may be considered as approximately constant, what allows Eq. (4.11) to be integrated by using the average value <γ>. Then, by integrating both members of Eq. (4.11) with respect to *f* one finds:

$$\beta = \beta_0 \left(\frac{f}{f_0} \right)^{-1-<\gamma>} , \tag{4.12}$$

where β_0 and f_0 are reference values. Because $\partial(\Delta P)/\partial f > 0$, <γ> is generally positive. On the other hand, for arteries that supply tissues without lymphatic vessels $i_{lymph} = 0$, and also tissues exist for which the reflection coefficient σ is very high, while permeability K_{ci} (and then a_k) approaches zero. This is the case of the brain for which $a_k \approx 0$, and σ_{ci} is very high, and therefore a less pronounced decrease in arterial distensibility with heart rate is expected to occur with the carotid as compared with the arteries that supply tissues with small values of reflection coefficient (e.g. the skeletal muscle).

4.4 The cases of the carotid and radial arteries

Very few data of arterial distensibility at various heart rates are found in the literature. To our knowledge only Giannattasio and co-workers [6] published in 2003 data of distensibilities of the carotid and radial arteries at heart rates of 63, 90 and 110 b.p.m. (beats per minute). In the following we will analyse those data in the light of Eq.(4.12).

As regards the value of <γ> respecting the carotid and radial arteries we observe that the first one supplies the brain whose tissues have a very high refection coefficient due to the highly selective barrier that separates the circulating blood from the extracellular fluid in the brain. Conversely, the radial artery that supplies the skeletal muscle in the arm presents a much lower reflection coefficient.

Table 4.1 Arterial distensibilities at various heart rates from ref. [6] and parameter <γ> [see. Eq. (4.12)].

Heart rate (b.p.m.)	**Distensibility (1/(mm Hg) ×10^{-3})**	
	radial artery	**carotid artery**
63	0.69	1.40
90	0.36	1.13
110	0.30	0.91
<γ>	**γ= 0.531**	**γ= -0.254**

On the other hand, by using the definition of characteristic radial frequency $\hat{\omega}=1/kx^2$ [see Eq. (4.7)], together with the pertinent values taken from ref. [20] it is found that the characteristic frequencies of the carotid and radial arteries, $\hat{f}=\hat{\omega}/2\pi$, are 3020 and 736 b.p.m., respectively. As a consequence the ratio $\hat{f}/f$ corresponding to the carotid artery is about 40 times larger than that of the radial artery.

By using the data of [6], and fitting Eq. (4.12) to a logarithmic scale: $\ln(\beta/\beta_0)\simeq-(1+<\gamma>)\ln(f/f_0)$, one obtains the values of <γ> shown on Table 4.1.

These results deserve scrutiny in the light of Eq. (4.11a).

4.4.1 Radial artery

The radial artery supplies the skeletal muscle in the arm, which has high permeability K_{ci} ($a_k\approx0.5$), and very low reflection coefficient, σ_{ci}, therefore from Eq.(4.11a) we conclude that <γ> must be positive. Moreover i_{lymph} may be significant in the arm thus adding a positive contribution to the already positive value of <γ>. The value $<\gamma>=0.531$ found for the radial artery from patient data [6] is in accordance with the tendency anticipated from Eq. (4.11a).

4.4.2 Carotid artery

This artery supplies the brain, whose capillaries due to the Blood-Brain Barrier have very low permeability K_{ci}, (and then $a_k \approx 0$) together with a very high reflection coefficient σ_{ci}. On the other hand, as referred above, though small drainage might occur by a special system [17], the brain has no lymphatic vessels, then $i_{lymph} = 0$. By taking into account all these aspects we conclude that <γ> must be negative. In addition, the ratio $\hat{f}^2 / f^2$ is high therefore modulating the value of <γ>, accordingly. By using data from the same ref. [6] we found $< \gamma >= -0.254$, which due to the properties of the carotid artery is also in accordance with Eq. (4.11) and Eq. (4.12).

In this way, the reduction of arterial distensibility with heart rate appears as the result of the adjustment of the artery that supplies some part of the body to the particular features of the microcirculatory tree (end capillaries) and the interstitial space in that part of the body. Mircoli and co-workers [10] found that in rats "in predominantly elastic-type arteries, the stiffening effect of tachycardia is exerted independently of sympathetic modulation". In fact, and in line with this finding no external control by any system external to the arterial tree (e.g. the sympathetic nervous system) was invoked in the analysis above developed, rather the effect of arterial stiffening with heart rate sprang of the continuity of blood flow [Eq. (4.8)] together with the coefficients that characterize the exchanges that occur between the end capillaries and the interstitial space [Eq. (4.9)].

4.5 Conclusions

In this paper, we showed that the effect of reduction of arterial distensibility with heart rate may be understood based on the physical properties of the arterial tree that supplies some tissues and the particular properties of blood exchanges between the end capillaries and the interstitial space in those tissues. The parameters that are relevant for the analysis are arterial wall distensibility, permeability and reflection coefficients of the end capillaries, which together account for arterial vasoactivity.

It was found that reduction of arterial distensibility with heart rate was greater in arteries that supply blood to end capillaries with high permeability coefficients

together with low reflection coefficients. This trend was confirmed through the use of data of distensibilities at the heart rates of 63, 90 and 110 b.p.m respecting the radial and carotid arteries.

In line with findings that showed that the effect of arterial stiffening with heart rate was virtually independent of sympathetic modulation, the present results showed that the assumption of continuity of blood flow together with the coefficients that characterize the exchanges between the end capillaries and the interstitial space may be sufficient to explain the observed effects.

Conflict of interest statement

The authors declare no conflict of interest.

Acknowledgement

The authors acknowledges the funding provided by the CGE, under the contract with FCT (the Portuguese Science and Technology Foundation), Pest/OE/CTE/UI0078/2014.

Appendix A. Supporting information

Supplementary data associated with this article can be found in the online version at http://dx.doi.org/10.1016/j.jbiomech.2014.07.025 .

References

[1] C. Mavroudis, “To pulse or not to pulse”, *The Annals Thor. Surg.* 25 259-271 (1978).

[2] K. M. Taylor, W. H. Bain, K. G. Davidson, M. A. Turner, “Comparative clinical study of pulsatile and non-pulsatile perfusion in 350 consecutive patients”, Thorax 37, 324-330 (1982).

[3] C. Silva, A.H. Reis, “Structure and adaptation of arteries to pulsatile flow e the case of the ascending aorta”, Med. Phys. 41 (6) 063701 (2014)

[4] R. Asmar, A. Scuteri, J. Topouchian, A. M. Brisac, J. Maldonado, L. Cloarec, M. Safar, “Arterial distensibility and circadian blood pressure variability”, Blood Pressure Monitoring, V.1, n. 4, 333-338, (1996).

[5] Y. L. Liang, C. D. Gatzka, X. J. Du, J. D. Cameron, B. A. Kingwell, A. M. Dart, “Effects of heart rate on arterial compliance in men” *Clinical and Experimental Pharmacology and Physiology*, 26, 342–346 (1999).

[6] C. Giannattasio, A. Vincenti, M. Failla, A. Capra, A. Cirò, S. De Ceglia, G. Gentile, R. Brambilla, G. Mancia,"Effects of Heart Rate Changes on Arterial Distensibility in Humans", *Hypertension*, 42:253-256 (2003).

[7] A. Pitcher, P. Leeson, C. Forfar, C. Trevitt, J. M. Francis, S. Neubauer, S. E. Petersen Aortic distensibility decreases during exercise in normal volunteers, *Journal of Cardiovascular Magnetic Resonance*, 12(Suppl 1), P136 (2010).

[8] T. Koskinen, M. Juonala, M. Kähönen, A. Jula, L. Keltikangas-Järvinen, J. Viikari, I. Välimäki, T. Laitinen, O. T. Raitakari, "Relations between carotid artery distensibility and heart rate variability:The Cardiovascular Risk in Young Finns Study", *Autonomic Neuroscience: Basic and Clinical*, 161, 75–80 (2011).

[9] C. Chrysohoou, V. Metaxa, J. Skoumas, S. Lagoudakou, S. Athanassopoulou, H. Kosyfa, E. Oikonomou, J. Felekos, D. Tsiachris, C. Masoura, C. Pitsavos, C. Stefanadis, Aortic artery distensibility shows inverse correlation with heart rate variability in elderly non-hypertensive, cardiovascular disease-free individuals: the Ikaria Study, *Heart Vessels,* 28:467–472 (2013).

[10] L. Mircoli, A. A. Mangoni, C. Giannattasio, G. Mancia, A. U. Ferrari, "Heart Rate-Dependent Stiffening of Large Arteries in Intact and Sympathectomized Rats" *Hypertension*, 34, 598-602 (1999).

[11] I. B. Wilkinson, N. H. Mohammad, S. Tyrrell, I. R. Hall, D. J. Webb, V. E. Paul, T. Levy, J. R. Cockcroft, "Heart Rate Dependency of Pulse Pressure Amplification and Arterial Stiffness", *American Journal of Hypertension*, 15, 24–30 (2002).

[12] K. Aizawa, M. E. Mendelsohn, T. J. Overend, R. J. Petrella, "Effect of Upper Body Aerobic Exercise on Arterial Stiffness in Older Adults", *Journal of Aging and Physical Activity*, 17, 468-478 (2009).

[13] B. A. Kingwell, G L. Jennings, K. L. Berry, A. M. Dart, J. D. Cameron, "Arterial compliance increases after moderate-intensity cycling", *Am. J. Physiol.* 273 (*Heart Circ. Physiol.* 42 : H2186– H2191 (1997).

[14] K. D. Currie, S. G. Thomas, J. M. Goodman, "Effects of short-term endurance exercise training on vascular function in young males", *Eur. J. Appl. Physiol*., 107: 211–218 (2009).

[15] Jae-Bin Seo, Woo-Young Chung, Sang-Hyun Kim, Myung-A Kim, Joo-Hee Zo "Immediate impact of exercise on arterial stiffness in Humans", *World Journal of Cardiovascular Diseases*, 3: 40-45 (2013).

[16] A. Farrugia, "Albumin Usage in Clinical Medicine: Tradition or Therapeutic?", *Transfusion Medicine Reviews*, 24, No, 1: 53-63 (2010).

[17] A. E. Taylor, Capillary fluid filtration. Starling forces and lymph flow, *Circulation Research*, 49, 3: 557-575 (1981).

[18] J. Seifter, D. Sloane, A. Ratner, *Concepts in Medical Physiology*, Lippincott Williams, & Wilkins, Baltimore, p.162 (2005).

[19] A. H. Reis, Constructal Theory: From Engineering to Physics, and How Flow Systems Develop Shape and Structure, *Appl. Mech. Rev*. 59, (5) 269-282 (2006).

[20] P. Reymond, F. Merenda, F. Perren, D. Rüfenacht and N. Stergiopulos, "Validation of a one-dimensional model of the systemic arterial tree", *Am. J. Physiol. Heart Circ. Physiol.*, 297: H208–H222 (2009).

CHAPTER 5

Conclusions

This thesis presents a model of a pulsatile flow system of branching channels that was developed with the purpose of studying some particular characteristics of human arterial tree. A RC model was designed to represent each channel of the branching tree, and to define the global impedance of a dichotomous branching. Based on the idea that flow structures exhibiting several branching levels are thought to perform optimally – Constructal Theory - the minimization of global flow impedance of the flow tree under constant global volume, was carried out. Scaling laws of diameters of a pulsatile flow system emerge, which in the limit of continuous flow (absence of pulse frequency) successfully reduce to Murray's Law of consecutive diameters. It was found that these optimal scaling varies with both pulse frequency and channel wall's distensibility, and is also dependent on the asymmetry factor of the daughter channels. In addition, if the process of minimization of flow impedance under constant pressure head is also considered, scaling laws for channel lengths emerge, following a law similar to that of channel diameters. This general model, based on the processes of minimization allows understanding the influence of the coefficients of distensibility of parent and daughter channels, because the results suggested that the channel with lower relative distensibility must have its diameter increased in order to perform optimally. Therefore the distensibility of blood vessels is a parameter of great importance in the characterization of arterial tree performance.

Then, the developed model was applied to the arterial tree. Based on the Navier-Stokes equation for a unidirectional flow, a scaling analysis was performed demonstrating that an RC model is suitable to represent behaviour of arterial vessels. The modulus of flow impedance of a cylindrical channel was considered in the analysis

of the arterial impedance behaviour with age. The study was carried out with respect to the ascending aorta, descending aorta and carotid artery, for which data was available, and results clearly demonstrates that arterial impedance tends to decrease with age for the assessed arteries. In the aortas the decrease is more pronounced during growth (first two decades of life). Due to lack of data the study respects to the period between birth and the age of 30. Regarding the carotid artery, it was found that its impedance tends to decrease linearly until the age of 40, keeping decreasing until the 7^{th} decade. These results of arterial impedances also show that the ascending aorta presents lower impedance as compared to the descending and carotid arteries, in agreement with what would be expected in a flow tree; daughter vessels (descending aorta and carotid artery) present impedances with higher values when compared with their parent vessel (ascending aorta). It is clear that these results are in agreement with Constructal Law which states that: "For a finite-size system to persist in time (to live), it must evolve in such a way that it provides easier access to the imposed currents that flow through it." This means that flow architectures evolve in such a way that under the existing constraints, the distribution of flow resistances change in time in order to achieve minimum global flow resistance, and which was just observed in the aortas and carotid artery. It appears that Nature (human arterial tree in this case) might have developed some internal mechanism of optimization.

The analysis of the variation of arterial impedance with heart rate showed that changes in arterial impedance were not significant. Even when variation of distensibility with pulse frequency, (which is significant in some arteries), is considered, the same conclusions were achieved.

Still on the vascular tree, the optimal scaling laws for diameters and lengths for a pulsatile flow system were used in order to assess if the human arterial tree is optimized from the point of view of blood flow performance. The idea was to examine what would be the optimal dimensions of some arterial segments as if they were free to change their morphologies to optimize performance, leaving out the real set of constraints of the circulatory system, namely the body size, the location of organs, or temporary needs of some part of the organism. The results showed that the optimal diameters of daughter vessels are mostly close to those observed.

With respect to channel length scaling, in general no such agreement was observed. Nevertheless, some ambiguity exists with respect to channel lengths listed in the literature. It was verified that some particular daughter channels have long parent vessels, usually exhibit small branches and therefore do not fully comply with the conditions of applicability of the scaling law that followed from the RC model. Indeed, there was some uncertainty in the calculation involving data of arterial segments lengths, especially for longer segments such as the case of the femoral artery whose proximal diameter (5.2 mm) and distal diameter (3.8 mm) differ considerably, strongly suggesting the presence of many small branches along the artery. This aspect may also justify the few agreements observed in length scaling, more precisely in the comparison of daughter length estimated values to the real ones. As discussed before there are many constraints in the human body that are not taken in account in the process of deduction of optimal scaling laws, and that might explain some discrepancies. However, we conclude that the comparison of real values with optimal values can be taken as for identifying the arteries where blood flow is not optimized and where hemodynamics might affect their performance.

In addition, the analysis focused on the ascending aorta and aortic arch. It was found that the sum of the optimal length of these two arteries is estimated to be 143.8 mm, which is much higher than the real one (60 mm). This discrepancy in those values, might help explain the results of the study by Sugawara and co-workers who showed that between 20 and 80 years in healthy subjects the average length of the ascending aorta (defined from aortic annulus to apex arch) tends to increase from 44 to 98 mm. This aspect further confirms the thought that the arterial flow system tends to optimize its performance in time. In this case, the ascending aorta that is in a cavity slightly constrained by nearby tissues is quite free to morph, actually. This tendency of natural flow system to change its configuration in time, is observed in many animate and inanimate systems, and ads credit to Constructal theory.

Finally, the model was used to explain the observed reduction of arterial distensibility with pulse frequency that is verified in some arteries. A non-specific artery together with the ensemble of tissues fed by that artery was analysed. Flow continuity was assumed in the sense that the blood flow current within the artery equals the sum of

all microcurrents flowing in the related tissues. To model the microcurrents which exist between the capillaries and the interstitial fluid in which blood bathes the tissues, Starling equation was take in account. Under the consideration of optimal performance, a formula emerges relating changes in arterial distensibility with heart rate, and also with some particular characteristics of microcirculation such as permeability and reflection coefficients of the end of the capillaries. The formula was tested in carotid and radial arteries, with data of distensibilities at heart rates of 63, 90 and 110 b.p.m.. The radial artery supplies the skeletal muscle in the arm, has high permeability and very low reflection coefficient, while carotid artery that supplies the brain, has capillaries with very low permeability and a very high reflection coefficient due to the Blood-Brain Barrier. The results suggested that the phenomena of reduction of arterial distensibility with heart rate, was more pronounced in arteries supplying blood to end capillaries, with both high permeability and low reflection coefficients. From the results it was concluded that the assumption of continuity of blood flow (at capillary level) together with the special properties of the exchanges that occur between the end capillaries and the interstitial space may be enough to explain the different degree of distensibility reduction, in agreement with findings that showed that this effect is independent of sympathetic modulation.

In this work the general purpose was of observing the trends of some physiological properties of the arterial tree, and then giving a physical explanation based on an optimized model of a pulsatile flow system. This model was developed in the light of Constructal Theory, which was applied for the first time to the circulatory system, adding to other fields of application of this theory.